https://doi.org/10.5607/en21004
Exp Neurobiol. 2021 Apr;30(2):120-143.
pISSN 1226-2560 • eISSN 2093-8144

Original Article

Experimental Neurobiology

Tumor Spheroids of an Aggressive Form of Central Neurocytoma Have Transit-Amplifying Progenitor Characteristics with Enhanced EGFR and Tumor Stem Cell Signaling

Hye Young Shin[1], Kyung-Seok Han[2†], Hyung Woo Park[1†], Yun Hwa Hong[3†], Yona Kim[1†], Hyo Eun Moon[1], Kwang Woo Park[1], Hye Ran Park[1], C. Justin Lee[2], Kiyoung Lee[1], Sang Jeong Kim[3], Man Seung Heo[4], Sung-Hye Park[5], Dong Gyu Kim[1] and Sun Ha Paek[1,6,7*]

[1]Department of Neurosurgery, Seoul National University College of Medicine, Seoul 03082, [2]Center for Cognition and Sociality, Institute for Basic Science, Daejeon 34126, [3]Department of Neurophysiology, Seoul National University College of Medicine, Seoul 03082, [4]Smart Healthcare Medical Device Research Center, Samsung Medical Center, Seoul 06351, [5]Department of Pathology, Seoul National University College of Medicine, Seoul 03082, [6]Ischemic/Hypoxic Disease Institute, Cancer Research Institute, Seoul National University College of Medicine, Seoul 03082, [7]Clinical Research Institute, Seoul National University Hospital, Seoul 03082, Korea

Central neurocytoma (CN) has been known as a benign neuronal tumor. In rare cases, CN undergoes malignant transformation to glioblastomas (GBM). Here we examined its cellular origin by characterizing differentiation potential and gene expression of CN-spheroids. First, we demonstrate that both CN tissue and cultured primary cells recapitulate the hierarchal cellular composition of subventricular zone (SVZ), which is comprised of neural stem cells (NSCs), transit amplifying progenitors (TAPs), and neuroblasts. We then derived spheroids from CN which displayed EGFR+/MASH+ TAP and BLBP+ radial glial cell (RGC) characteristic, and mitotic neurogenesis and gliogenesis by single spheroids were observed with cycling multipotential cells. CN-spheroids expressed increased levels of pluripotency and tumor stem cell genes such as *KLF4* and *TPD5L1*, when compared to their differentiated cells and human NSCs. Importantly, Gene Set Enrichment Analysis showed that gene sets of GBM-Spheroids, EGFR Signaling, and Packaging of Telomere Ends are enriched in CN-spheroids in comparison with their differentiated cells. We speculate that CN tumor stem cells have TAP and RGC characteristics, and upregulation of EGFR signaling as well as downregulation of eph-ephrin signaling have critical roles in tumorigenesis of CN. And their ephemeral nature of TAPs destined to neuroblasts, might reflect benign nature of CN.

Key words: Central neurocytoma, Tumor spheroids, Subventricular zone, Neural stem cell, Transit-amplifying cells, Radial glia cells, Gene Set Enrichment Analysis

INTRODUCTION

Central neurocytoma (CN) is a peculiar type of brain tumor that occurs most frequently in young adults, developing in the subventricular zone (SVZ) area of the lateral ventricle. They were initially classified as Organization (WHO) grade I lesions, but in 1993 CNs were upgraded to WHO grade II lesions when it was recognized they could exhibit more aggressive behavior [1] and recurrences

Submitted March 15, 2021, Revised March 26, 2021, Accepted March 26, 2021

*To whom correspondence should be addressed.
TEL: 82-2-2072-2350, FAX: 82-2-744-8459
e-mail: paeksh@snu.ac.kr
†These authors contributed equally to this article.

[2]. Malignant neoplasms such as glioblastoma (GBM), in rare case, have been reported to arise from dedifferentiation of CN in an area distal to the SVZ [3] in the previous study, in which histological diagnosis of the tumor located in the right lateral ventricle was CN whereas two tumors of the left temporal lobe were GBM, and the specimen of GBM showed CN histology. This clinical observation indicates that CN itself has inter-tumor heterogeneity observed between patients with the same tumor type due to genetic variability, heterogeneity in microenvironment [4]. Similarly, previous findings that despite being a neuronal tumor, CN cells have the capacity to differentiate into both neurons and glia in an *in vitro* culture environment [5, 6] corresponds well with the some case of relatively aggressive form of CN.

However, it has been unclear which cells within the CN tumor mass are responsible for tumor initiation and maintenance. Hassoun et al. [7] suggested that CN may originate from small gray nuclei of the septum pellucidum, which appear to be the site of tumor attachment, whereas von Deimling et al. [8] hypothesized that CN originates postnatally from the remnants of the subependymal germinal plate of the lateral ventricles. Similarly, Sim et al. hypothesized that CN derives from a neoplastic GFAP+ cell that undergoes selective expansion when removed to culture, and which is able to regenerate itself and form new neuroblasts [5]. However, the latter study was limited by the use of serum in the culture conditions: to maintain neural stem cells (NSCs) in an undifferentiated state, they must be grown in serum-free media [9]. The persistence of germinal regions and the presence of NSCs and transit amplifying progenitors (TAP) in the adult mammalian brain has suggested that tumor cells may arise from cells other than mature neural cells [10]. Indeed, brain tumor stem cells have been shown to be involved in the initiation and propagation of several types of brain tumors, namely: GBM (CD133+) [11], which is the most frequent primary intraparenchymal neoplasm in the elderly; medulloblastomas (MB) (CD133+) [12], which has the highest incidence in children; and ependymomas (EP) (CD133+, Nestin+, and BLBP+) [13]. The SVZ has been shown to be a source for tumor stem cells that initiate gliomagenesis [14]. SVZ astrocytes (Type B cells) have been identified as NSCs in the mouse [15, 16] and adult mammalian brain [17]. Type B cells/NSCs have ultrastructural characteristics of brain astrocytes and express GFAP [15]. Importantly, in human, Middeldorp et al., showed that the adult SVZ is indeed a remnant of the fetal SVZ, which develops from radial glial cell (RGC). Furthermore, the study provides evidence that GFAP-delta can distinguish actively proliferating Type B cells/NSCs in SVZ [18]. Dividing GFAP-delta+ Type B cells/NSCs give rise to type C cells/TAPs [16, 18], a population of rapidly dividing, immature-appearing cells. The Type C cells, which are likely TAPs, express OLIG2 [19], MASH (ASCL1) [19], EGFR [20], SOX2 [21]. Type C cells/TAPs in turn produce type A cells, the neuroblasts which express TUJ1 and the PSA-NCAM [22-24].

In light of the anatomical origin of CN origin and its phenotype, we hypothesized that CN has neuroblast characteristics and originates from NSCs or TAPs in the SVZ. We first isolated CN-spheroids from CN-differentiated cells, and showed that tumor spheroids have TAP and RGC characteristics, and generate both neuron and astrocyte based on immune-histochemical and electrophysiological examinations. We then performed a comparative transcriptomic analysis of CN-spheroids compared to CN-differentiated cells and human NSCs, and found the tumor spheroids showed increased expression of genes for TAP, RGC, pluripotency, and tumor stem cell compared to these other cell types. Gene set enrichment analysis (GSEA) algorithm also showed enrichment of tumor spheroids-specific gene signatures in CN-derived tumor spheroids compared to CN-differentiated cells and SVZ-NSCs. In addition, intuitive neurogenesis signaling was detected in CN-differentiated cells and SVZ-NSCs.

MATERIALS AND METHODS

Experimental design

We obtained tissues of CNs from surgeries of three patients (N=3), and then we performed primary cultures of CN tissues. To define cellular composition of CN tissues and primary cells, three biological replicates (N=3) from different patients were analyzed, and tumor spheroids were isolated from differentiated cells for characterization (RT-PCR and immunostaining) and electrophysiological study. Single tumor sphere RT-PCR was done to confirm that all individual spheres express tumor stem cell markers and to rule out any artifact which can arise from mixed population-derived RNA analysis. One of the three samples yielded a notable number of tumor spheroids for microarray. Other samples also made tumor spheroids, but the amount of RNA was not optimal for the microarray. This reflects that rare case report of malignancy of CN. As shown in Fig. 1b, a CN tissue that has a bigger size of tumor mass on MRI imaging made a robust number of tumor spheroids. For gene expression analysis, we compared CN-differentiated cells (N=1) and CN-spheroids (N=1) to defined specific genes, expressed on CN-spheroids. Gene expression of CN-spheroids were also compared with fetal SVZ-derived NSCs (N=1) to detect overlapped and differential expression. For a comparative study between samples, expression data was standardized using z-score transformation.

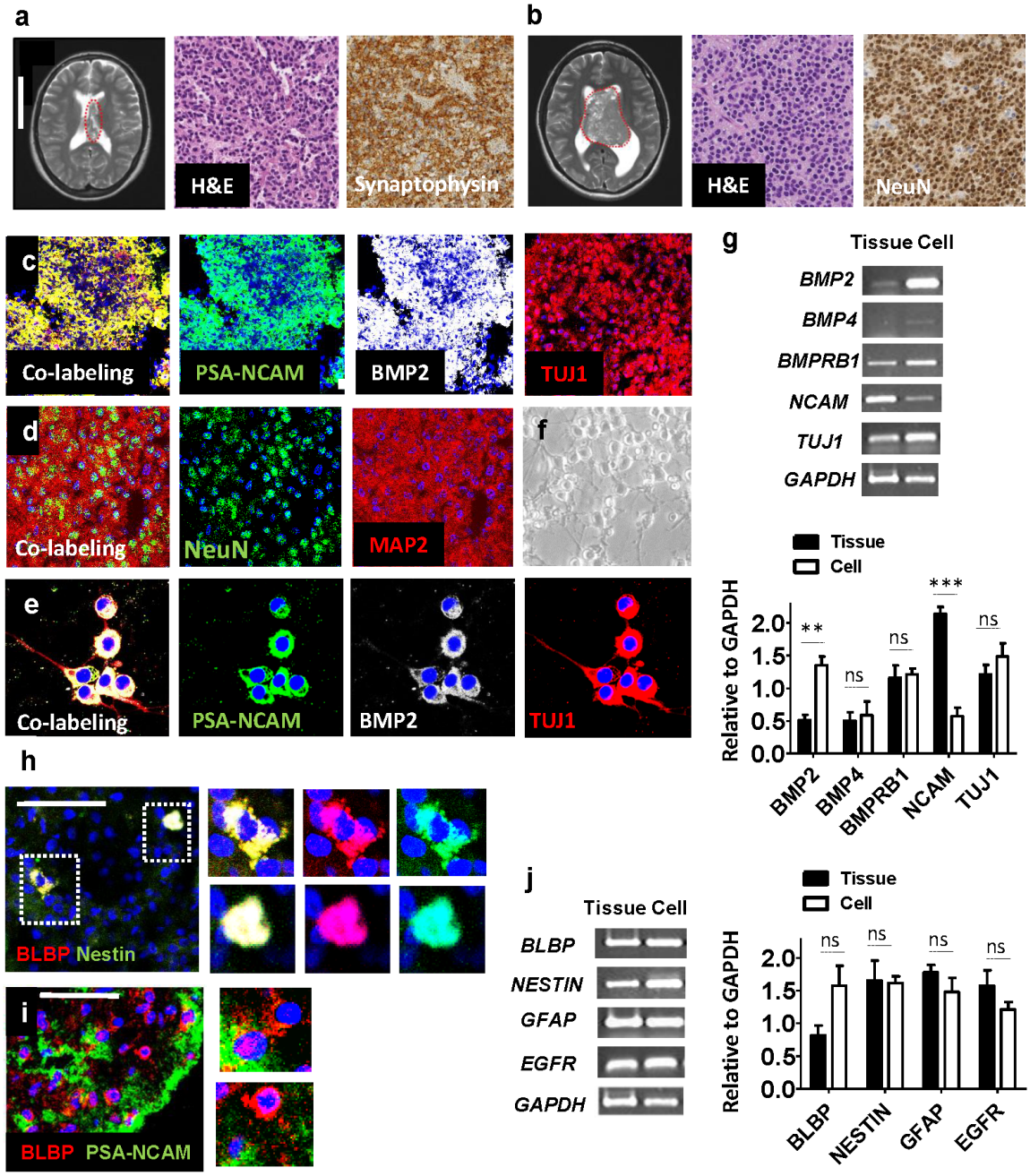

Fig. 1. Neuroblast-like characteristics of CN. (a, b) Representative images of MRI (Left), H&E (Middle), and Synaptophysin or NeuN (Right) of two patients among three patients. A T2 weighted brain MRI shows an inhomogeneous mass lesion in the left lateral ventricle of Patient 1 (a) and both lateral ventricle of Patient 2 (b). Patient 2 has much bigger size of tumor mass when compared to Patient 1. Red dotted line indicates CN tumor mass. H&E of the Patient 1 (a) and 2 (b) shows sheet of monotonous rounded cells with rounded nuclei. Synaptophysin (a) and NeuN (b) is robustly positive in tumor cells of the patients. (c, d) CN tissue with immunofluorescence staining of PSA-NCAM, BMP2, and Tuj1 (c) and NeuN and MAP2 (d). Each first panel indicates co-localization. (e) Immunofluorescence staining of CN-derived cells grown in ITSFn media shows localization of PSA-NCAM, BMP2 and Tuj1 representing neuroblast character. (f) CN-derived cells have round shape without mature neuronal structures. (g) Up: RT-PCR of CN tissue and CN-differentiated cells shows expression of BMP2, BMP4, BMPR1B, NCAM, Tuj1, and GAPDH. Bottom: Densitometry measurement of each genes relative to *GAPDH* in tissue and cell. F: 10.77, DFn: 4, $p<0.001$; Row factor has significant effects. (h) A few cells in CN tissue are Nestin+/BLBP+ representing RGC. (i) CN tissue has a mixed population of BLBP+ cells, BLBP+/PSA-NCAM+, and PSA-NCAM+ cells. (j) Left: RT-PCR of CN tissue and CN-differentiated cells detected expression of BLBP, Nestin, GFAP, and GAPDH. Right: Densitometry measurement of each genes relative to GAPDH. F:2.06, DFn:1 $p=0.1461$ no effect. Original full-length images of g and j are presented in Supplementary Fig. 3S. Scale bar 6 cm (a), 50 μm (c) 20 μm (e) 100 μm (h, i) 20 μm. All data presented as mean +/- S.D. Two way ANOVA followed by Bonferroni correction and t-test analysis was done. A p value of <0.01 (**), 0.001 (***), and ns: not significant was used to denote statistical significance. Three biological samples (N=3) were used for the experiments.

https://doi.org/10.5607/en21004

Human samples

Use of human CN tumor samples (N=3) for primary cultures in this study was approved by the Institutional Review Board (IRB) of Seoul National University Hospital (IRB approval C-0710-040-223). The human CN, normal ependymal tissues were obtained from the Brain Bank of Seoul National University Hospital, as approved by IRB of Seoul National University Hospital (IRB approval H-0B05-036-243). Fetal SVZ tissues (N=1) was obtained from inevitable abortion because of fatal diseases, and those tissues were primary cultured, as approved by IRB of Seoul National University Hospital (IRB approval H-0408-130-002). All methods were performed in accordance with the relevant guidelines and regulations of IRB board of Seoul National University Hospital. All the patient samples were obtained after obtaining written informed consent.

Primary culture of CN tissue

Methods for establishment of primary cultures for this study were approved by the Institutional Review Board (IRB) at Seoul National University Hospital (IRB No; C-0710-040-223). CN tissues from three patients (N=3) were mechanically dissected and enzymatically dissociated to single-cell suspensions using papain (Sigma-aldrich, St. Louis, MO) and DNase I (Sigma-aldrich) as described previously [25]. The cells were then suspended in DMEM/F12 (Invitrogen, Carlsbad, CA) supplemented with 5 μg/ml insulin (Sigma-aldrich), 50 μg/ml transferrin (Sigma-aldrich), 30 nM selenium chloride (Sigma-aldrich), and 5 μg/ml fibronectin (Sigma-aldrich) (ITSFn medium), and DMEM-FBS20%.

Immunostaining and fluorescent in situ hybridisztion (FISH)

Immunohistochemistry and immunocytochemistry [25, 26] were performed as described previously. Briefly, the cells were rinsed with PBS, fixed with 4% paraformaldehyde for 30 minutes at room temperature, and washed three times with PBS. Tissues were post-fixed by ice-cold 4% paraformaldehyde in PBS (pH 7.4) for one day at 4℃, and then cryoprotected overnight in the same fixative supplemented with 25% sucrose. The tissues were embedded in OCT compound (Sakura Finetek, Inc., Torrance, CA), and frozen at -70℃ with dry ice. Sections (14 lm thick) were cut with a cryotome (Leica Microsystems, Wetzlar, Germany).

CN were analyzed by FISH for 1p and 19q on paraffin-embedded (FFPE) tissue sections to verify its diagnosis as describe in the previous study [27]. Dual, fluorescent-labelled DNA probes are used to detect 1p and 19q loci within the interphase nuclei of individual glioma cells from FFPE tissue sections transcribed on to unstained slides. Changes in the 1p and 19q probe signals compared with controls are used to determine the presence of 1p/19q-co-deletion.

List of antibodies

Primary antibodies used in this study are Nestin rabbit IgG (AB5922, 1:500, Millipore Sigma, Carlsbad, CA, USA); GFAP mouse IgG (IF03L, 1:1000, Millipore Sigma) and rabbit IgG (04-1062, 1:1000, Millipore Sigma); Human nuclei Millipore mouse IgG (MAB1281, 1:500, Millipore Sigma); BLBP rabbit IgG (ABN14, 1:500, Millipore Sigma); GFAP-delta rabbit IgG (AB9598, 1:500, Millipore Sigma); MAP2 rabbit IgG (AB5622, 1:500, Millipore Sigma) and mouse IgG (05-346, 1:500, Millipore Sigma); Tuj1 mouse IgG (MAB1637, 1:500, Millipore Sigma); PSA-NCAM mouse IgG (MAB5324, 1:500, Millipore Sigma); Sox2 rabbit IgG (ab75627, 1:500, Abcam, Cambridge, UK); NeuN mouse IgG (MAB377, 1:500, Millipore Sigma); EGFR Rabbit IgG (ab32562, 1:500, Abcam, Cambridge, UK). All secondary antibodies are Goat anti-Mouse IgG (H+L) Cross-Adsorbed Secondary Antibody, Alexa Fluor 488 (A-11001, 1:600, Invitrogen, Carlsbad, CA, USA); Goat anti-Rabbit IgG (H+L) Cross-Adsorbed Secondary Antibody, Alexa Fluor 488 (A-11008, 1:600, Invitrogen); Goat anti-Mouse IgG (H+L) Cross-Adsorbed Secondary Antibody, Alexa Fluor 568 (A-11004, 1:600, Invitrogen); Goat anti-Rabbit IgG (H+L) Cross-Adsorbed Secondary Antibody, Alexa Fluor 568 (A-11011, 1:600, Invitrogen).

Confocal microscopy

Fluorescently immunolabeled sections were analyzed on a Meta confocal microscope (model LSM 510; Carl Zeiss MicroImaging, Inc., Jena, Germany) equipped with four lasers (Diode 405, Argon 488, HeNe 543, and HeNe 633). Each channel was separately scanned using a multitrack PMT configuration to avoid crosstalk between fluorescent labels. Cells were mounted with antifading solution containing 4'-6-diamidino-2-phenylindole (DAPI; H-1200, Vector Laboratories Burlingame, CA, USA), and observed under a confocal microscope (Carl Zeiss MicroImaging).

RT-PCR

Total RNA was isolated from cells that had been cultured with either ITSFn medium or DMEM-FBS), using an RNeasy mini kit (Qiagen, GmbH, Germany). First-strand cDNA synthesis was carried out by random priming of the total RNA using a random primer mixture (Invitrogen) and reverse transcriptase with superscript 3 (Invitrogen). All designed primers (Bioneer, Republic of Korea) were screened using BLAST (Basic Local Alignment Search Tool) to ensure specificity of binding. Primers were used at a concentration of 250 nM. The PCR program entailed 10 min of the 9494T Basic Local Alignment Search Tool to ensure specificity of binding. The PCR program was as follows: 10 min 94℃ pre-run, 30 s at 94℃, 30 s at 55℃, 2 min at 72℃ for 35 cycles, and 10

Table 1. Oligonucleotide primers and PCR conditions used for RT-PCR

Gene	Forward	Reverse	Product size (bp)
NESTIN	AGGATGTGGAGGTAGTGAGA	TGGAGATCTCAGTGGCTCTT	266
BLBP	CGCTCCTGTCTCTAAAGAGGGG	TGGGCAAGTTGCTTGGAGTAAC	594
BMPRIB	CATGCTTTTGCGAAGTGCAG	CAGGCAACCCAGAGTCATCC	197
MASH1	CCAACTACTCCAACGACTTG	GAAAGCACTAAAGATGCAGG	194
NCAM	GTCCTGCTCCTGGTGGTTGTG	CCTTCTCGGGCTCCGTCAGT	264
GFAP	CTGTTGCCAGAGATGGAGGTT	TCATCGCTCAGGAGGTCCTT	382
BMP2	TCAAGCCAAACACAAACAGC	ACGTCTGAACAATGGCATGA	200
BMP4	AAAGGGGCTTCCACCGTAT	CCGCTGTGAGTGCTTAG	386
hTERT	TGACACCTCACCTCACCCAC	CACTGTCTTCCGCAAGTTCAC	95
SOX2	CCCCCGGCGGCAATAGCA	TCGGCGCCGGGGAGATACAT	448
GAPDH	AGCTGAACGGGAAGCTCACT	TGCTGTAGCCAAATTCGTTG	297
CD133	TGGCAACAGCGATCAAGGAGAC	TCGGGGTGGCATGCCTGTCATA	633
EGFR	AACTGTGAGGTGGTCCTTGG	AGCTCCTTCAGTCCGGTTTT	231
MAP2	GGGATTAGCAGTAACCCACG	AGGCCATCTGTCCAAAGTCA	224
NF200	GCAGACATTGCCTACC	TCA CTC CTT CCG TCA CCC	349
TUJ1	ACTTTATCTTCGGTCAGAGTG	CTCACGACATCCAGGACTGA	97

min 72℃ post-run. No products were amplified in water. All the primer sequences are listed in Table 1.

Electrophysiology

CN cells were cultured as monolayers on 12 mm glass coverslips coated with poly-L-lysine (Sigma). External solution contained (in mM): 150 NaCl, 10 HEPES, 3 KCl, 2 $CaCl_2$, 2 $MgCl_2$, 22 sucrose, 10 glucose; pH was adjusted to 7.4 and osmolarity to 325 mOsm. The solution to fill the electrodes was composed of (mM) 140 K-gluconate, 0.5 $CaCl_2$, 1 $MgCl_2$, 5 EGTA, 10 HEPES, 4 Mg-ATP and 0.3 Na_3-GTP. Whole cell patch recordings were obtained from CN-differentiated cells in voltage clamp or current clamp configuration using a multi-clamp 700B (Axon instruments, Union City, CA, USA) and patch pipette of 4~7 MΩ resistance. The solution to fill the electrodes was composed of (mM) 140 K-gluconate, 0.5 CaCl2, 1 MgCl2, 5 EGTA, 10 HEPES, 4 Mg-ATP and 0.3 Na3-GTP with 0.5% biocytin for morphological analysis.

Calcium imaging

Cells were loaded in 5 mM Fura 2-AM (Molecular Probes, Eugene, OR) and 0.01% pluronic acid in HEPES-buffered salt solution (HBSS) for 45 min at 37uC, and then unloaded in HBSS for another 15 min. Cells were plated onto poly-L-lysine coated 12 mm coverslips. Coverslips with Fura 2-AM loaded cells were then transferred to a perfusion chamber on the stage of an upright microscope (Olympus BX50, Japan). Cells were illuminated by a Xenonlamp and observed with a 40X UV water-immersion objective lens (Olympus, Tokyo, Japan). For Fura 2-AM excitation, the shutter and filter wheel (polychrome-IV; TILL-Photonics, Martinsried, Germany) were controlled by Axon Imaging Workbench (AIW) software 2.1 (Axon Instruments, Foster City, CA) to provide sequential illumination at two alternating wavelengths, 340 and 380 nm. Fluorescence of Fura 2-AM was detected at an emission wavelength of 510 nm. Video images were acquired using an intensified CCD camera (LUCA; Andor, UK). Fluorescence emission ratios following excitation at 340 and 380 nm were calculated by dividing averaged pixel values in circumscribed regions of individual responding cells in the field of view. The values were exported from AIW to Origin 8.0 for additional analysis and plotting. The composition of the HBSS was (in mM); NaCl, 137; KCl, 5; MgSO4, 0.9; CaCl2, 1.4; NaHCO3, 3; Na2HPO4, 3;Na2HPO4, 0.6; KH2PO4, 0.4; glucose, 5.6; and HEPES, 20; pH 7.4. For the depolarization conditioning, Ca2+ imaging were performed in HBSS containing high K+ (133 mM K+ with substitution of Na+).

Microarray analysis

After hybridization, the chips were stained and washed in a GeneChip Fluidics Station 450. After the final wash and staining step, the microarray arrays were scanned using Affymetrix Model 3000 7G scanner and the image data was extracted through Affymetrix GeneChip Command Console software 1.1. For the normalization, Robust Multi-Average algorithm implemented in Affymetrix Expression Console software 1.1 was used. Use of human CN tumor samples (Biological replicates, N=3) for primary cultures in this study was approved by the Institutional Review Board (IRB) of Seoul National University Hospital (IRB approval C-0710-040-223). Attributing to its benign characteristics of CN, only one sample among those three was able to make robust number of tumor spheroids. Other sample also made tumor spheroids, but the amount of RNA was not optimal for the microarray. We

https://doi.org/10.5607/en21004

compared CN-differentiated cells (N=1) and CN-spheroids (N=1) to defined specific genes, expressed on CN-spheroids. Gene expression of CN-spheroids were also compared with Fetal SVZ-derived NSCs to detect overlapped and differential expression. For a comparative study between samples, expression data was standardized using z-score transformation. The GEO accession numbers for the gene expression and comparative genomic data used in this article are GSE42670 'Comparative transcriptomic analysis of central neurocytoma-derived tumor spheres as compared to its differentiated cells and fetal SVZ-derived neural stem cells'. For a normal control we used "GSM469410" from the public GEO database (http://www.ncbi.nlm.nih.gov/geo/).

GSEA analysis

We used GSEA [28] utilizing Molecular Signatures Database (MSigDB) [29] to determines whether an a priori defined set of genes (The False Discovery Rate (FDR)<0.25, p<0.01) shows statistically notable differences between CN-spheroids in comparison with CN-differentiated genes and SVZ-NSCs. For the analysis, we utilized category C2 among the MSigDB gene sets. Category C2 is curated gene sets from online pathway databases, publications in PubMed, and knowledge of domain experts. The FDR is calculated by comparing the actual data with 1000 Monte-Carlo simulations. The density of modified genes in the dataset is computed by the NES (Normalized Enrichment Score) with the random expectancies, and then it is normalized by the number of genes found in a given gene cluster.

Engraftment of cells

All procedures for animal experiments were approved by the IACUC (#07212) at Clinical research institute, Seoul National University Hospital. Experiments were performed in accordance with NIH guidelines. We assessed whether ITSFn-cultured cells are bipotential *in vivo* by evaluating their fate after engraftment to three immune-deficient NOD-SCID mice (male; N=3). CN cells (1×10^5) and SVZ-derived NSCs (1×10^5) were transplanted four weeks after primary culture to assess their lineage potential after transplantation (1×10^5 cells per ml) along the anterior-posterior axis into the target brain at these coordinates: from the bregma, 2 mm anteriorly, 3 mm laterally and to 5 mm depth. The cells were live-stained with DiI (Invitrogen) delivered by an infusion pump at 0.5 ml/min. The needle was left in situ for 2 min post-injection before being slowly removed. The recipients were sacrificed and fixed four weeks after transplantation.

Quantification and statistical analysis section

For the quantitative analysis, a similar threshold was set for all images (three slices per sample) of *in vitro* CN-derived cells and mice tissues cells on which CN-derived cells are transplanted. Five regions of interest (ROIs) were randomly selected in the different regions of the images, and the area of specific immunoreactivity was measured using an image analyzer (Image-Pro Plus, Media Cybernetics Co., Silver Spring, MD). Statistical analysis was performed using GraphPad Prism 5. All data are presented as the mean+SD. Statistical significance was determined using unpaired two tailed t test, One-Way and Two-Way ANOVA followed by Bonferroni correction and t-test. Statistical details (p value, F, and degree of freedom (Df) are provided in Figure legends. A p value of <0.05 (*) or 0.01 (**), and 0.001 (***) was used to denote statistical significance.

Data availability statement

All the microarray data is available on GEO database. The GEO accession numbers for the gene expression and comparative genomic data used in this article are GSE42670, which includes four sample, GSM2977251: CN-differentiated cells, GSM2977252: CN-tumor spheres, and GSM2977253: Fetal-SVZ-derived NSCs.

RESULTS

The majority of CN cells display neuroblast characteristics

CN tumor masses are located in the SVZ of the patients as shown on representative MRI (magnetic resonance imaging) images (Fig. 1a, b). These tumors are diagnosed as CN based on its location and immunohistochemistry, in which H&E shows sheet of monotonous rounded cells with rounded nuclei, and Synaptophysin and NeuN are robustly positive in tumor cells of CN (Fig. 1a, b). In addition, FISH results show that two red and two green signals are evident in CN tissues, which implies no deletion of chromosome 1p and 19q (Fig. 2s). No complete co-deletion of short arm of chromosome 1 (1p) and the long arm of chromosome 19 (19q) (1p/19q co-deletion) shows typical characteristics of CN.

We detected expression of PSA-NCAM and Tuj1 (Fig. 1c) and light expression of NeuN and MAP2 (Fig. 1d), which suggests that most cells within CN tumors are not fully matured neurons. BMP2, PSA-NCAM, and Tuj1 were expressed in CN tissue sections (Fig. 1c) and CN-primary cells in ITSFn media, which promoted survival of NSCs at 1 week after culture (Fig. 1e). The majority of CN cells are round in shape in original tumor tissues (Fig. 1c, d) and primary cell population (Fig. 1f, e) without typical mature neuronal morphology. Semi-quantitative RT-PCR revealed that *BMP2*, *BMPR1B*, *NCAM*, and *TUJ1*, but not *BMP4*, were expressed in CN tissues and its differentiated cells (Fig. 1g). This phenotype is consistent with neuroblasts [22] supporting the

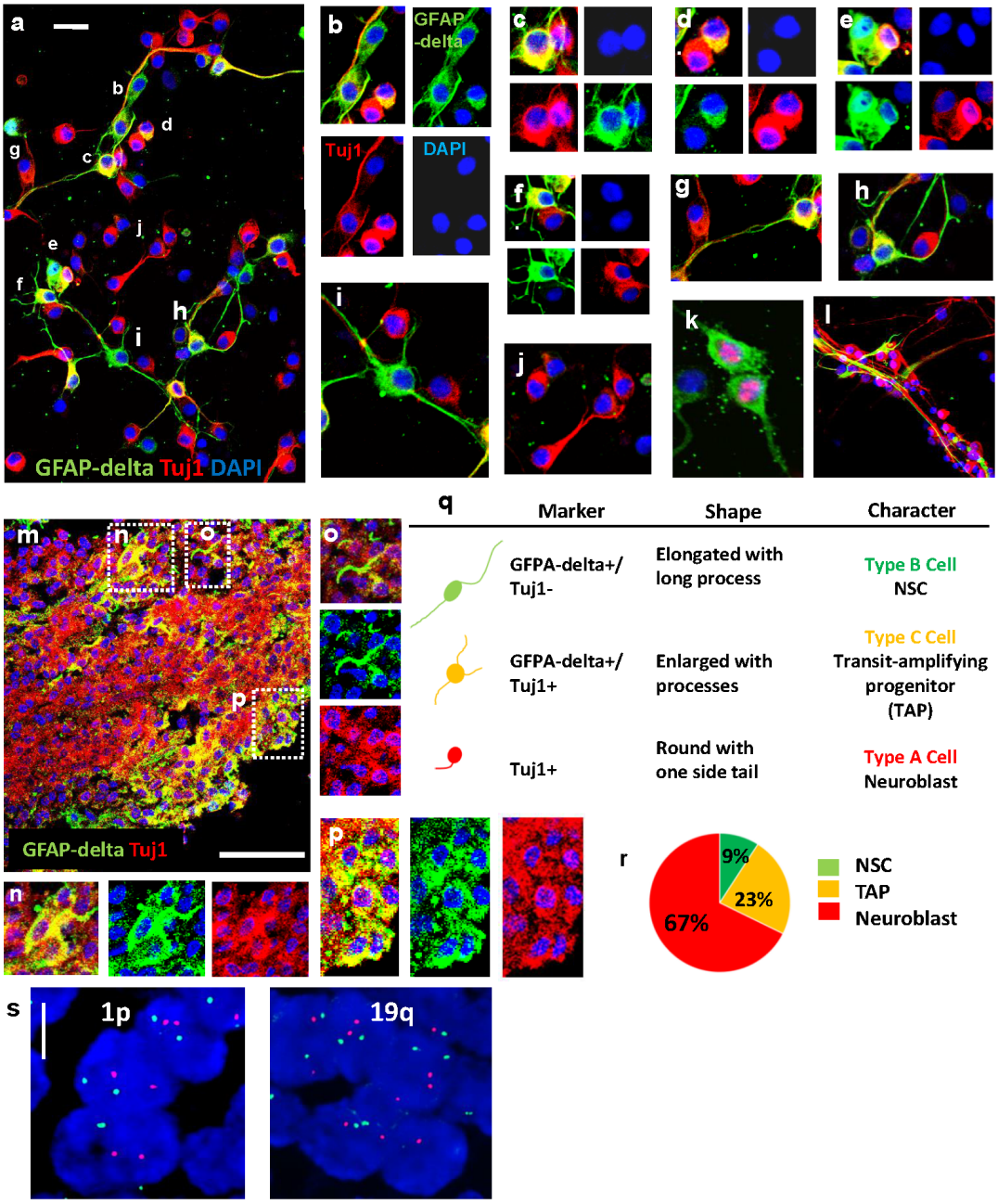

Fig. 2. SVZ-neurogenic cellular composition of CN-derived cells and CN tissue. (a) Immunofluorescence staining of CN-differentiated cells at 1 week, showing localization of GFAP-delta+ (Green), and Tuj1+ cells (Red), and GFAP-delta+/Tuj1+(Green/Red) at one week after culture. (b) Immunofluorescence staining of neurogenic RGC cells (GFAP-delta+) showing morphology and arrangement indicative of newly divided cells. (c~f) Immunofluorescence staining of GFAP-delta+/Tuj1+ cells and Tuj1+ cells, showing asymmetrical divisions. (g~i) Tuj1+ cells localized and migrated along the fiber of GFAP-delta+/Tuj1+ (g, h) and GFAP-delta+ cells (i). (j) Example of Tuj1+ neuroblasts, which comprise the major population of CN. (k) Ki67 indicates mitotic and twin-like GFAP-delta+ cells. (l) The basal processes of GFAP-delta+/Tuj1+ cells were wrapped around Tuj1+ neuroblasts at 3 weeks after culture. (m) Immunofluorescence staining of CN tissue, showing localization of GFAP-delta+, GFAP-delta+/Tuj1+, and Tuj1+ labeled cells. (n) GFAP-delta+ cells from CN tissue, showing long processes similar to RGC. (o) TAP-like GFAP-delta+/Tuj1+ cells showing several processes proximal to Tuj1+cells. (p) Immunofluorescence staining of CN tissue showing clustered GFAP-delta+/Tuj1+ cells resembling daughter neuroblasts (Tuj1+). (q) Characteristics of three kinds of cells including GFAP-delta+ Type B, GFAP-delta+/Tuj1+ Type C, and Tuj1+ Type A cells. (r) Percentage of each type of cells (GFAP-delta+ NSC, GFAP-delta+/Tuj1+ TAP, Tuj1+ Neuroblast) in the population of CN: Type B (9.167±1.878 N=3), Type C (22.67±2.333 N=3), and Type A cells (67.47±2.784 N=3). (s) Representative FISH images carried out on these two tumors. Left: FISH images of 1p36 (red signal) as a target and of 1q24 (green signal) as a reference probe. Right: 19q13.3 (red signal) as a target and of 19p13 (green signal) as a reference. Two red and two green signals are evident, which implies no deletion of chromosome 1p and 19q. Scale bars, 50 μm (a) 100 μm (m) 10 μm (s). Three biological samples (N=3) were used for the experiments.

https://doi.org/10.5607/en21004

hypothesis that CN cells have neuroblast characteristics. Interestingly, a few BLBP+/Nestin+ RGC like cells (Fig. 1h), numerous BLBP+/PSA-NCAM+ intermediate cells or PSA-NCAM+/Tuj1 neuroblasts (Fig. 1i) were observed in the CN tissue, suggesting that PSA-NCAM+/Tuj1+ cells might originate from BLBP+ cells in CN. These results are supported by gene expression of *BLBP*, *Nestin*, *GFAP* (Fig. 1j) and Tuj1 (Fig. 1g) in CN tissue and its primary cells at 1 week after dissociation.

CN has SVZ-hierarchal neurogenic cell composition

We next performed immunocytochemistry to examine the identity and distribution of neurogenic cell types present in CN. GFAP-delta, a marker for the SVZ-NSCs [18], and Tuj1 were immunostained on CN-primary cells (Fig. 2a~l) and CN tissue (Fig. 2m~p). In particular, the heterogeneity of the neurogenic cell types results in a non-uniform distribution of subpopulations across and within disease sites of CN tissue (Fig. 2m~p). We observed that, in the ITSFn-cultured CN primary cells at 1 week (Fig. 2a), CN tissue (Fig. 2m), and normal subependymal tissue (Fig. 3a), three kinds of cells were present: NSC-like GFAP-delta+, TAP-like GFAP-delta+/Tuj1+; GFAP-delta+/PSA-NCAM+; and neuroblast-like Tuj1+; PSA-NCAM+ cells. In contrast, we detected no TAP-like GFAP-delta+/Tuj1+ cells in the SVZ of fetal brain tissue (Fig. 3d). Importantly, GFAP-delta+ cells were predominantly located in the vicinity of the SVZ area and did not co-label with Tuj1 in the SVZ of fetal brain tissue, consistent with the immature status of fetal cells, compared to adult cells in the SVZ. This observation is supported by the previous studies as following. It has been reported that the transitional state of sibling TAPs express low levels of GFAP and DCX [30], and that GFAP+ cells differentiate to form intermediate Hu+(neuronal marker)/GFAP+ progenitors [31]. Similarly, an earlier study reported the presence of GFAP+/MASH1+ adult NSCs and MASH+/DCX+ adult TAPs in adult SVZ, which indicates a more mature state for adult NSC compared to fetal NSCs [32].

We also observed that in CN primary cells and tissue, NSC-like GFAP-delta+ cells (Fig. 2b, i, n) grew considerably in size exhibiting large bipolar-oriented processes. TAP-like GFAP-delta+/Tuj1+ cells (Fig. 2c, f, g) have an enlarged cell body with several processes. In contrast, the neuroblast-like Tuj1+ cells are round in shape with one side tail with the smallest size of cell body. (Fig. 2j). This observation is correlated with the previous report which shows a highly significant difference between the size of astroglial NSCs (largest) and either TAPs or neuroblasts (smallest) [30]. Interestingly, some of NSC-like GFAP-delta+ cells and TAP-like GFAP-delta+/Tuj1+ cells were localized in close opposition with a "twin-like" morphology (Fig. 2b, e), suggesting that NSC-like GFAP-delta+ cells divide asymmetrically to self-renew (GFAP-delta+), and to generate TAP-like GFAP-delta+/Tuj1+ cells. Ki67 expression shows that GFAP-delta+ cells are mitotic (Fig. 2k). Similarly, TAP-like GFAP-delta+/Tuj1+ cells and postmitotic neuroblast-like Tuj1+ cells were also located adjacent to each other, implicating these cells may also undergo asymmetric cell divisions reminiscent of RGC (Fig. 2c, d, f). Consistent with that notion, the small nuclei attached to TAP-like GFAP-delta+/Tuj1+ cells in Fig. 2c suggest asymmetric divisions have occurred. Moreover, these GFAP-delta+/Tuj1+ cells are resembled with their daughter Tuj1+ cells (Fig. 2c, d, f). Interestingly, Tuj1+ cell and GFAP-delta+/Tuj1+ cell in Fig. 2g recapitulate a neuroblast migrating along a long RGC fiber. Majority of GFAP-delta+/Tuj1+ cells display bipolar morphology, extending long process that was interestingly reminiscent of RGCs in the brain, and Tuj1+ cells have a round shape with tails attached on the fiber (Fig. 2g, h). In the prolonged culture (3 weeks after culture), the basal processes of GFAP-delta+/Tuj1+ cells were wrapped around the bundles of Tuj1+ neuroblasts (Fig. 2l). This observation suggests that TAP-like GFAP-delta+/Tuj1+ cells may constitute the tumor stem cells in CN. In particular, mitotic –and its lineage differentiation resulted in the heterogeneity of the neurogenic cell types as a non-uniform distribution of subpopulations across and within disease sites of CN tissue (Fig. 2m~p). Clustered TAP-like GFAP-delta+/Tuj1+ cells (Fig. 2p) were also observed in CN tissue, and their morphology resembled with daughter neuroblasts (Tuj1+). Fig. 2q shows summarized observation of the neurogenic subpopulation of the CN and characteristic of each cell type including distinctive cellular morphology and phenotypic expression. NSC-like cells (GFAP-delta+) comprised significantly a small portion of the CN primary cells (9.167%±1.878 N=3, $p<0.05$ and $p<0.001$ by *t* test compared to TAP-like cell and daughter neuroblasts, whereas TAP-like cells (GFAP-delta+/Tuj1+) comprised 22.67%±2.333 N=3, and daughter neuroblasts (Tuj1+) comprised 67.47%±2.784 N=3 (Fig. 2r). Overall, our results support the concept that the CN cell population has hierarchical neurogenic components similar to the SVZ.

CN-derived tumor spheroids show TAP and RGC-like characteristics

We initially maintained CN-derived cells in two culture conditions: ITSFn, which is optimal for proliferation and maintaining non-differentiation; and DMEM-FBS, which promotes differentiation. During the first week, the cells were predominantly flattened and attached. At that point, tumor spheroids began to form, not only in ITSFn media but also, surprisingly, in the DMEM-FBS media (Fig. 4a). Among three patient CN tissues, one sample made a significant number of tumor spheroids than other two samples. CN tissue, which has a bigger size of tumor mass on MRI imaging

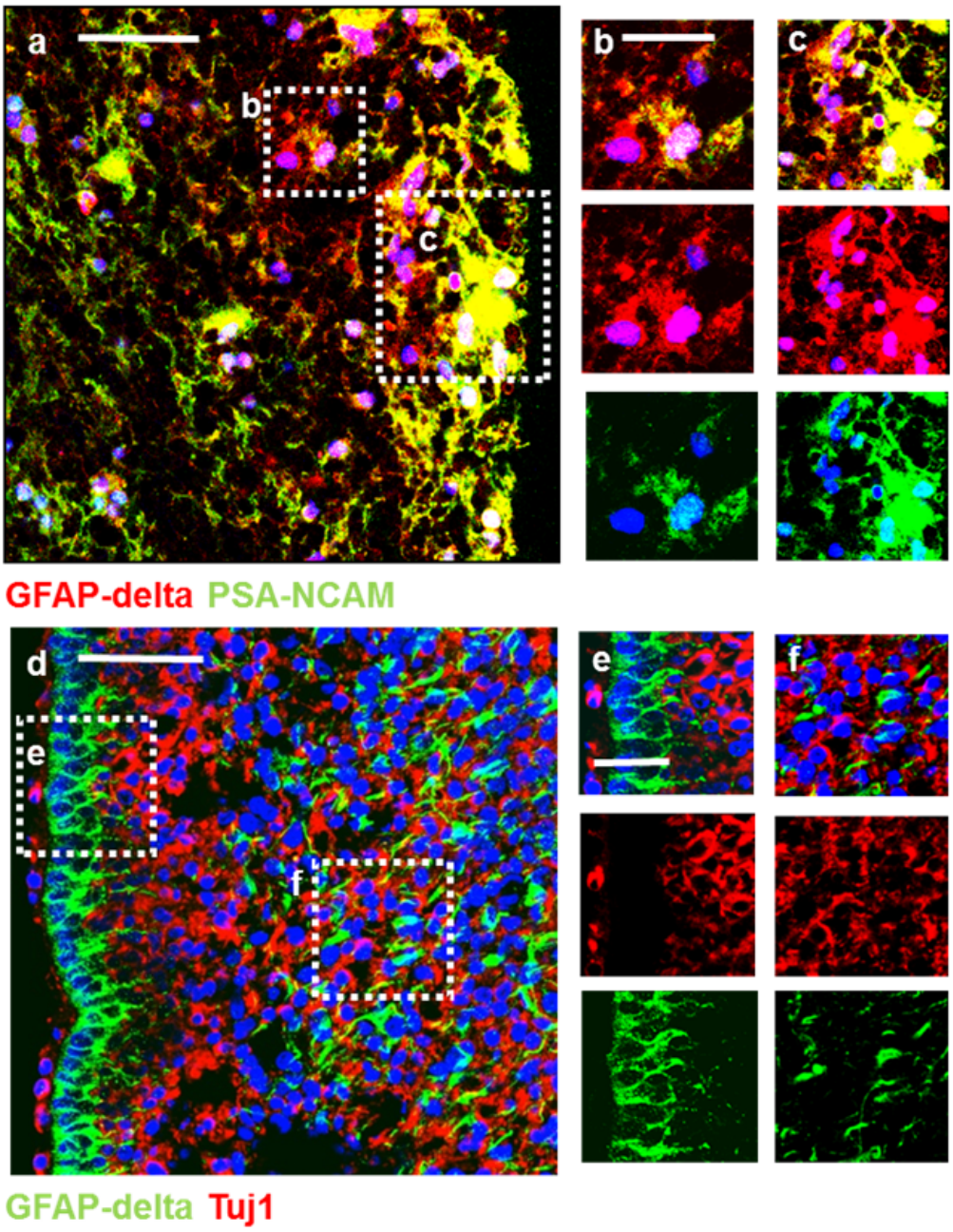

Fig. 3. Adult human ependymal and fetal SVZ tissue and has the same cell composition of CN. (a) Neurogenic radial glia-like cells (GFAP-delta+) and daughter neuroblasts (PSA-NCAM+) have small population, whereas intermediate progenitor-like cells (GFAP-delta+/PSA-NCAM+) have large portion in normal subependymal tissue. (b) Neurogenic RGC-like GFAP-delta+ cell divided asymmetrically to self-renew and to produce GFAP-delta+/PSA-NCAM+ cell in normal subependymal tissue. (c) TAP-like GFAP-delta+/PSA-NCAM+ cells have large portion in subependymal tissue. (d) Representative image for GFAP-delta and Tuj1 on human fetal SVZ tissue. (e, f) There is no GFAP-delta+/Tuj1+ cells GFAP-delta+ cells near SVZ on human fetal SVZ tissue. Scale bar, 100 μm (a, d) 50 μm (b, e). One enpendymal tissue (N=1) and fetal SVZ (N=1) were used for the experiments.

(Fig. 1b), made a robust number of tumor spheroids. To characterize properties of the CN-spheroids, we performed RT-PCR and IF on single tumor spheroids. We detected RGC makers, *GFAP*, *NESTIN*, and *BLBP*, in both fractions (Fig. 4b up), implicating an RGC origin for the CN-spheroids. Statistically, ITSFn-cultured CN-spheroids showed higher expression of *NESTIN*, *SOX2*, *EGFR*, and *hTERT* as compared to DMEN-FBS-cultured CN-spheroids (Fig. 4b bottom). TAP markers, MASH1, EGFR, and SOX were also detected in both spheroids (Fig. 4b). Neither fraction expressed *NF 200*, *MAP2*, and little *TUJ1* was expressed (Fig. 4b), indicating the

https://doi.org/10.5607/en21004

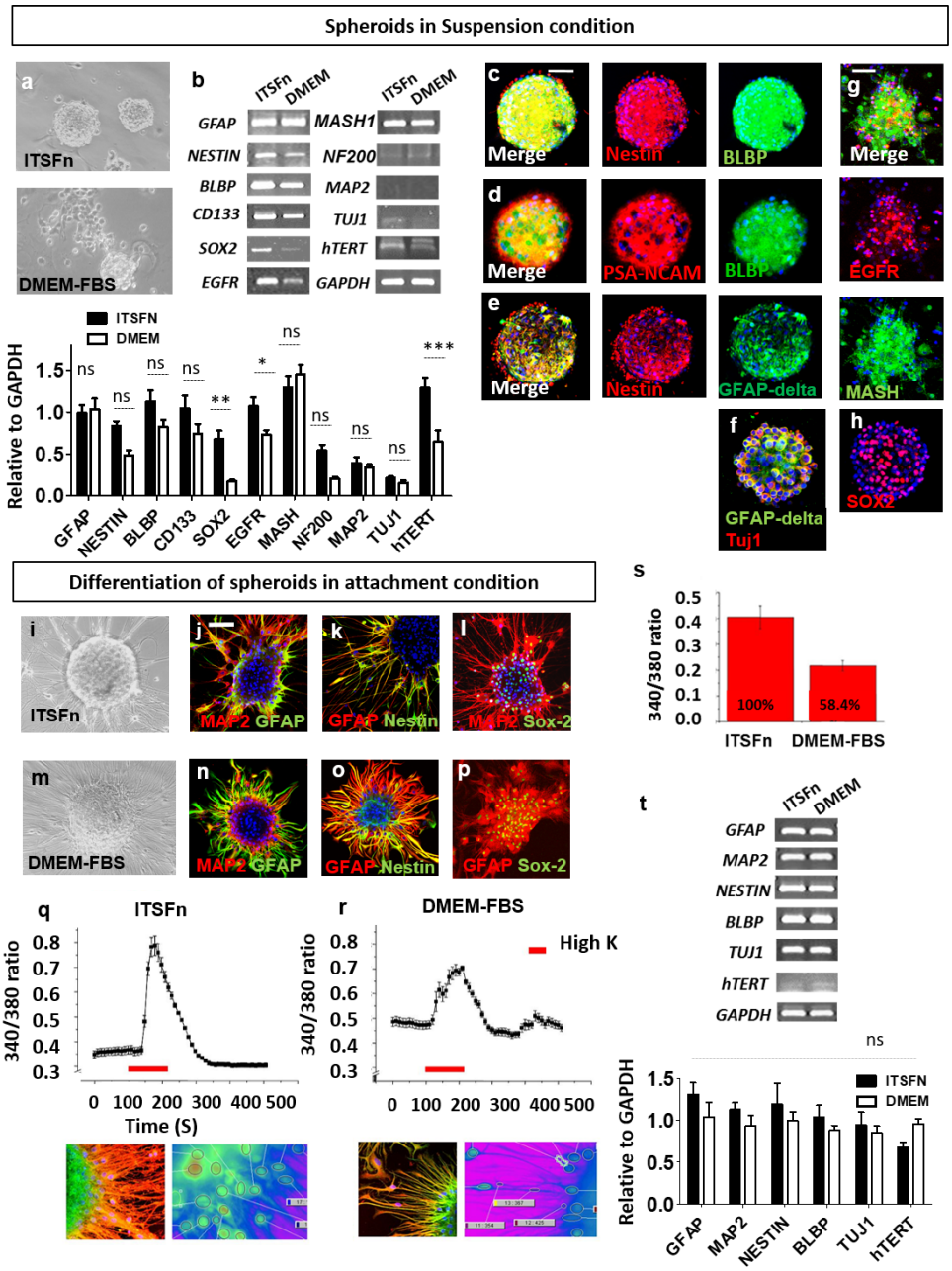

Fig. 4. TAP and RGC-like characteristics and bipotentiality of CN-spheroids. (a) Tumor spheroids formed in ITSFn and DMEM-FBS media. (b) Up: Representative images of RT-PCR shows expression of NSC makers: *GFAP*, *Nestin*, *BLBP*, *CD133*, *SOX2*, *hTERT*. In particular, ITSFn-derived CN-spheroids express higher level *Nestin*, *BLBP*, *CD133*, and *SOX2*. Bottom: Densitometry measurement of each genes relative to *GAPDH*. (c~h) Immunofluorescence staining of CN-spheroids. Nestin+/BLBP+(c), PSA-NCAM+/BLBP+(d), Nestin+/GFAP-delta+(e). GFAP-delta+/Tuj1+ shows mixed population of RGC and neuroblasts (f). TAP characteristics were confirmed by EGFR+/MASH+ cells (g), SOX2+ cells (h). (i, m) CN-spheroids were attached on the dish and cultured up to 4 weeks. Phase contrast view of ITSFn- (i) and DMEM-FBS-(m) cultured CN tumor sphere shows migration and differentiation of cells at the edge of the sphere. (j~l) CN-spheroids cultured in ITSFn differentiated mostly into neuronal cells (j). (n~p) DMEM-FBS media induced more glia differentiation of the CN-spheroids (n). (q, r) Ca2+ imaging (lower left panels) and immunofluorescence staining (lower right panels) of CN-spheroids cultured in ITSFn (left) and DMEM-FBS (right) media. Cells were pre-loaded with Fura 2. AM, washed and pre-incubated for at least 10 min prior to the addition of KCl (133 mM) for 60 sec. (s) The time of KCl addition is indicated by red. The level of Ca2+ responses to high K+ was almost two folds in CN-spheroids in ITSFn as compared to DMEM-FBS. Error bars indicate SEM. (t) Up: Representative images of RT-PCR shows expression of NSC makers: *GFAP*, *Nestin*, *BLBP*, *CD133*, *SOX2*, *hTERT*. Bottom: Densitometry measurement of each genes relative to *GAPDH*. Original full-length images of b and t are presented in Supplementary Fig. 3S. Scale bars, 100 μm (c, g, j). All data presented as mean +/- S.D. Two way ANOVA followed by Bonferroni correction and t-test analysis was done. A p value of <0.05 (*) or 0.01 (**), 0.001(***), and ns: not significant was used to denote statistical significance. Three biological samples (N=3) were used for the experiments.

cells were in a TAP-like immature transient state. The expression of human Telomerase (*hTERT*) was rarely detected in DMEN-FBS-cultured CN-spheroids but pronounced in ITSFn-cultured CN-spheroids (Fig. 3b). Both ITSFn- and DMEM-FBS-cultured CN-spheroids displayed mixed population of NSCs (Nestin+/BLBP+/GFAP-delta+), TAPs (BLBP+/PSA-NCAM+; GFAP-delta+/Tuj1+), as well as a few neuroblasts (PSA-NCAM+ or Tuj1+) in the periphery of spheroids (Fig. 4c~f). In particular, CN-spheroids shows immature transient state with merged expression of BLBP+/PSA-NCAM+ and GFAP-delta+/Tuj1+ (Fig. 4d~f). This observation is consistent with clustered cell population of GFAP+/Tuj1+ in CN tissue (Fig. 2p). Accordingly, CN-spheroids expressed representative markers of TAP, namely ALCL1 (MASH1), EGFR (Fig. 4g), and SOX2 (Fig. 4h) in consistent with the RT-PCR result (Fig. 4b). Taken together, these observations suggest that CN tissue contains RGC- and TAP-like tumor stem cells *in vivo*.

The bipotentiality of RGC-like CN-spheroids

The observation that tumor spheroids can be generated in cultures of CN-derived cells prompted us to examine whether these cells can generate both neurons and glia. Accordingly, to evaluate differentiation potency, CN-spheroids were attached on the plate, and cultured up to 4 weeks (Fig. 4i, m). We observed that differentiation began in the cells localized on the periphery of the spheroids, while cells localized to the interior of the sphere remained SOX2+ immature cells (Fig. 4l, p). Then individual cells migrated out from spheroids (Fig. 4i, m) and begun to differentiate to form MAP2+/Tuj1+ neurons or GFAP+ astrocytes (Fig. 4j, n). Some of the cell were still immature Nestin+ cells (Fig. 4k, o). Majority of ITSFn-cultured cells showed neuronal differentiation (Fig. 4j), and DMEM-FBS-cultured cells generated mostly astrocytes (Fig. 4n), both spheroids are potential though. In parallel, elevations in intracellular free Ca2+ concentration in response to high KCl was two folds higher in the cells migrating from the ITSFn-cultured colony when compared to DMEM-cultured colony (Fig. 4q~s). We performed single spheroid RT-PCR on each ITSFn-cultured colony and DMEM-FBS-cultured colony. *GFAP*, *MAP2*, and *TUJ1* expression was detected in both fractions, suggesting that both CN-spheroids are bipotential (Fig. 4t). Meanwhile, the detection of *NESTIN* and *BLBP* by RT-PCR, as shown in Fig. 4t, is attributed to the presence of Nestin+ cells (Fig. 4k, o). In that case, the persistence of mitotic neurogenesis and gliogenesis by single spheroids is consistent with the presence of cycling multipotential cells. Taken together, these observations suggest that CN tissue contains RGC- and TAP-like tumor stem cells *in vivo*.

In the prolonged culture up to 4 weeks, expression of MAP2 and NeuN decreased notably in DMEM-FBS-cultured cells, which resulted in widespread GFAP+ glia cells (Fig. 5a, b). Accordingly, DMEM-cultured cells had no changes in intracellular free Ca2+ concentration by membrane depolarization with high KCl (Fig. 5c). Meanwhile, in ITSFn-culture neural cells, expressions of MAP2 and NeuN (Fig. 5d, e) were maintained up to 8 weeks, and high KCl bathing solution for 60 sec increased intracellular free Ca2+ concentration (Fig. 5f). Neuron-like cells displayed rapid, reversible, >100% elevations in intracellular free Ca2+ concentration in response to high KCl, consistent with the activity of neuronal voltage-gated calcium channels (Fig. 5f), and it was blocked by 2 M nimodipine, a voltage-dependent calcium channel blocker (Fig. 5g). In addition, ITSFn-cultured cells was able to develop fast sodium currents and action potentials characteristic of eletrophysiologically competent neurons. Whole-cell patch-clamp recording was performed during current stimulation. CN-derived neurons in ITSFn showed action potentials by current steps of 20 pA (Fig. 5h). The action potentials were blocked by 0.5 M TTX (Fig. 5i). A total of 14 cells were recorded. Of these, 3 cells showed voltage-activated sodium ion currents. In addition, none of cells cultured in DMEM-FBS showed substantial current-induced sodium currents (Data not shown). Together, these results indicated that neurons arising from ITSFn-cultured CN cells developed mature electrophysiology functions, including both fast sodium currents and action potential. The biocytin solution was filled into the electrodes for morphological analysis, and these cells were confirmed as MAP2+ by immunostaining (Fig. 5j). Based on these observations, CN-derived cells have bipotential in response to different environmental niche.

GSEA indicated tumor stem cell features of CN-spheroids

GSEA [28] utilizing Molecular Signatures Database (MSigDB) [29] is a computational method that determines whether an a priori defined set of genes (FDR<0.25, p<0.01) shows statistically significant, concordant differences between two biological states. First, in comparison with CN-differentiated cells, CN-spheroids showed upregulation of gene sets in GBM cell lines displaying spherical growth (cluster-1) compared to those displaying semi adherent or adherent growth phenotype (cluster-2) (Fig. 6a) [33]. Gene sets of packaging of telomere ends (reactome) (Fig. 6b) and EGFR signaling (Fig. 6c) [34] were upregulated in CN-spheroids as well. These results are well correlated with the gene expression of *hTERT* and *EGFR* (Fig. 4b) and EGFR+ cells (Fig. 4g) in ITSFn-cultured CN-spheroids. In addition, CXCR chemokine receptor binding (Gene Ontology (GO)) (Fig. 6d) [35], KEGG glycine and serine and threonine metabolism (Fig. 6e) and KEGG steroid hormone biosynthesis (Fig. 6f) were enriched in CN-spheroids as compared to their differentiated cells. In particular, the serine,

https://doi.org/10.5607/en21004

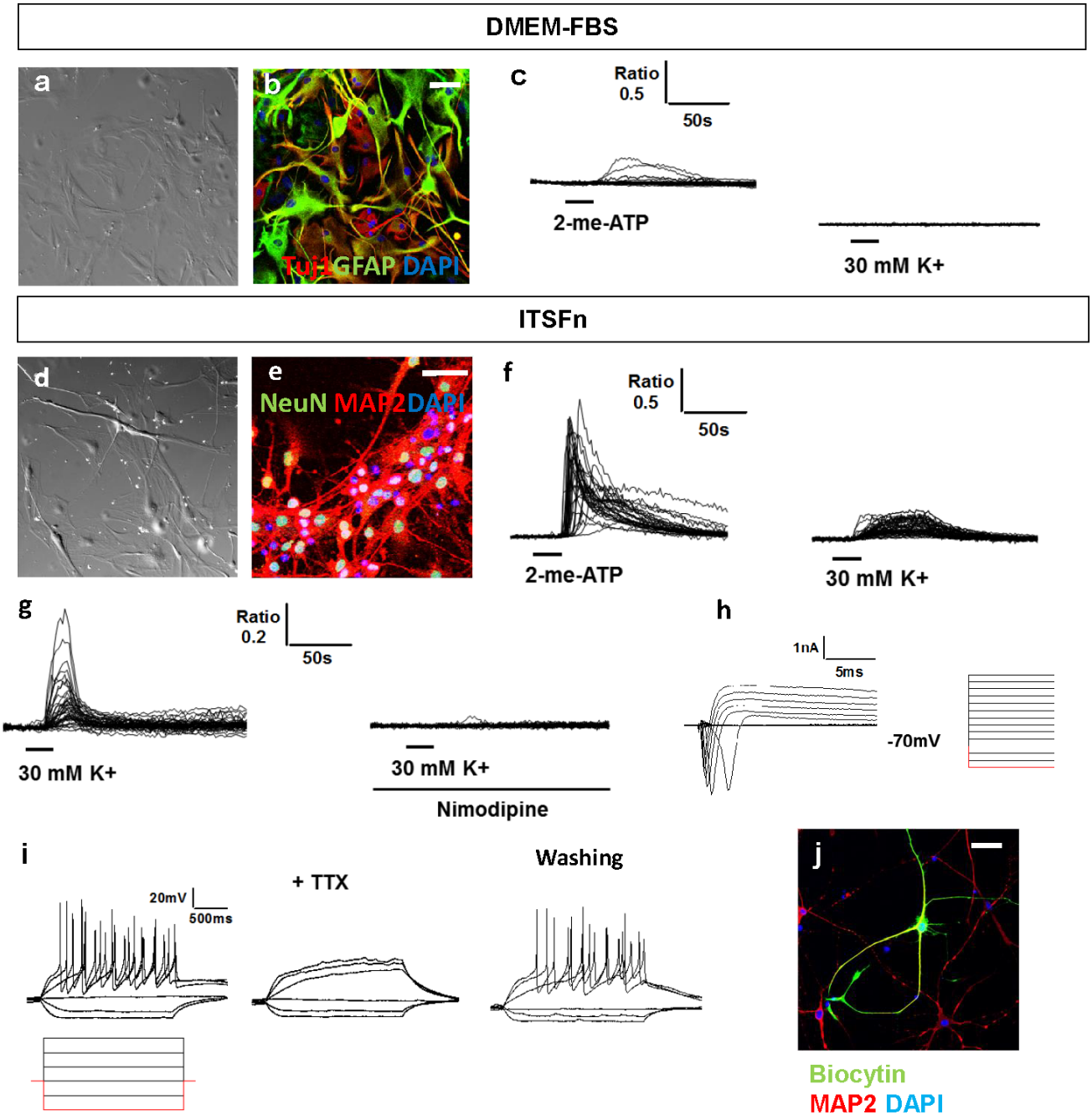

Fig. 5. Long-term culture of CN-differentiated cells show bipotential in response to different environmental niche. (a~c) Most of the cells matured into astrocytes in DMEM-FBS. No neuronal activity was observed in those astrocytes. (d~f) Fully matured neuronal cells (MAP2+; Red /NeuN+; Green) were observed in ITSFn media, and those neuronal cells showed high level of Ca2+ transient in response to high KCl. (g) Ca2+ response of cells in ITSFn media by 30 mM K+ in the absence or presence of 2 M nimodipine. (h) Whole cell recordings of CN-differentiated cells under voltage clamp held at -70 mV. Voltage steps of 10 mV were applied to the cell under voltage clamp. Each trace indicated a recording of different cells. (i) CN-derived neuroblasts matured into neuron for 4 weeks analyzed by current injection of 20 pA steps under current clamp. Action potentials were blocked by 0.5 uM TTX. Out of 14 cells, 3 cells showed action potentials. After TTX was washed off, action potentials were revived. (j) The biocytin solution was filled into the electrodes, and injected to the cells which show action potectial for morphological analysis, and these cells these cells were confirmed as MAP2+ by immunostaining. Scale bars, 50 μm (b, e, j).

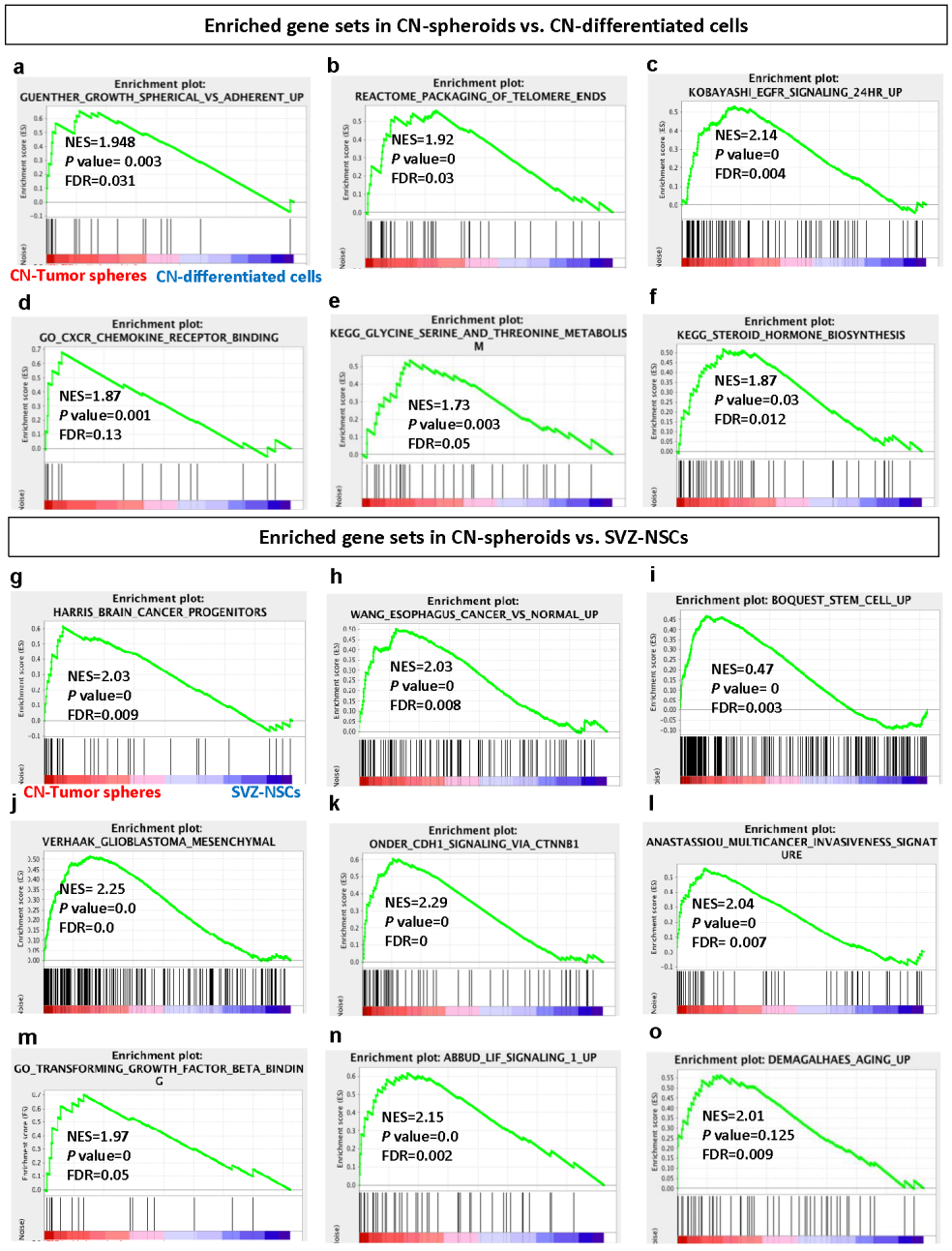

Fig. 6. GSEA algorithm shows that gene sets of tumor spheroid and NSCs are highly enriched in CN-spheroids in comparison with CN-differentiated cells and SVZ-NSC. In every thumbnail, the green curve represents the evolution of the density of the genes identified in microarray gene chip. The heat-map on the right shows where the gene expression is relatively high (red) or low (blue) for each gene in the indicated sample. (a~f) Enriched gene sets in CN-spheroids versus CN-differentiated cells. (a) GUENTHER_GROWTH_SPHERICAL_VS_ADHERENT_UP. (b) REACTOME_PACKAGING_OF_TELOMERE_ENDS. (c) KOBAYASHI_EGFR_SIGNALING_24HR_UP. (d) GO_CXCR_CHEMOKINE_RECEPTOR_BINDING. (e) KEGG_GLYCINE_SERINE_AND_THREONINE_METABOLISM. (f) KEGG_STEOROID_HORMONE_BIOSYNTHESIS. (g~o) Enriched gene sets in CN-spheroids vs. SVZ-NSCs. (g) HARRIS_BRAIN_CANCER_PROGENITORS: Genes from the brain cancer stem (cancer stem cell, CSC) signature. (h)WANG_ESOPHAGUS_CANCER_VS_NORMAL_UP: Up-regulated genes specific to esophageal adenocarcinoma (EAC) relative to normal tissue. (i) BOQUEST_STEM_CELL_UP: Genes up-regulated in freshly isolated CD31- (stromal stem cells from adipose tissue) versus the CD31+ (non-stem) counterparts. (j) VERHAAK_GLIOBLASTOMA_MESENCHYMAL: Genes correlated with mesenchymal type of glioblastoma multiforme tumors. (k) ONDER_CDH1_SIGNALING_VIA_CTNNB1. (l) ANASTASSIOU_MULTICANCER_INVASIVENESS_SIGNATURE: Invasiveness signature resulting from cancer cell/microenvironment interaction. (m) GO_TRANSFORMING_GROWTH_FACTOR_BETA_BINDING (Gene Ontology (GO): Interacting selectively and non-covalently with TGF-beta, transforming growth factor beta, a multifunctional peptide that controls proliferation, differentiation and other functions in many cell types. (n) ABBUD_LIF_SIGNALING_1_UP: Genes up-regulated in AtT20 cells (pituitary cancer) after treatment with LIF. (o) DEMAGALHAES_AGING_UP: Genes consistently overexpressed with age, based on meta-analysis of microarray data.

 https://doi.org/10.5607/en21004

glycine, one-carbon (SGOC) metabolic network is implicated in cancer pathogenesis metabolism [36].

Secondly, in comparison with SVZ-NSCs, CN-spheroids showed upregulation of gene sets of brain cancer progenitors (Fig. 6g) [37], specific to esophageal adenocarcinoma (EAC) relative to normal tissue (Fig. 6h) [38], stromal stem cells (Fig. 6i), mesenchymal type of GBM tumors (Fig. 6j) [39], CDH1 signaling via CTNNB1 (Fig. 6k) [40], invasiveness signature resulting from cancer cell/microenvironment interaction (Fig. 6l) [41], Transforming growth factor beta binding (Gene Ontology (GO) (Fig. 6m), and LIF signaling (Fig. 6n) [42]. In addition, when compared to SVZ-NSCs, genes consistently overexpressed with age [43] were upregulated in CN-spheroids in consistent with its older age in comparison with fetal cells (Fig. 6o).

Analysis of differentially expressed genes (DEGs) shows RGC & TAP characteristics of CN-spheroids

We next performed differential expression gene (DEG) analysis (Fig. 7 and 8) on CN-spheroids, CN-differentiated cells, and SVZ-NSCs, to compare expression of genes associated with cancer stem cells, pluripotency, tumor suppression, and cancer-related signaling pathways. Importantly, we found that CN-spheroids were upregulated in expression of the cancer stem cell-associated genes *CXCR12* [44], *CXCR4* [44], *CDK4* [45], *PCDHB7* [46], *AQP4* [47], *TPD52L1* [48], *ID1* [49], *ID3* [49], *CD44* [50], and *PDPN* [51], and the pluripotency-related genes *OCT4* [52], *NANOG*, *SOX2*, *KLF4*, and *CBX7* (Fig. 7b) [53], when compared to both CN-differentiated cells and SVZ-NSCs. Interestingly, *Cbx7* has been shown to maintain pluripotency by repressing lineage-specific genes such as *Cbx2* [53]. CN-spheroids showed a decrease, whereas, in the expression of the tumor suppressor-associated genes *MCM2* [54], *EPHB3* [55-57], and *EPHB4* [55-57], and the neuronal differentiation-related genes *FOXO3* [58], *CCND1* [34], *WNT7A* [59], *CDH2* [60], *CNTN1* [61], *SIRT1* [62], *CBX2* [53]. *ASPM* [63], and *INA* (Fig. 8) [64].

We also found that in comparison with CN-differentiated cells, both CN-spheroids and SVZ-NSCs showed upregulation of genes for RGC (*NOTCH3* [65], *FABP7* [66], *SLC1A3* [66], *DAB1* [67], *ERBB4* [68], and *VCAM* [69]), TAP (*OLIG1* [19], *OLIG2* [19], *ASCL1* [19], *SOX2* [21], and *EMX2* [70]), SVZ-stem cell (*CSPG2-VCAN*, *CSPG3-NCAN*, *CSPG5* [71], *HAS3* [72], *CDH1* (*E-cadherin*) [40], *FZD3* [73], and *AQP6*) (Fig. 7c). RGC gene upregulation is well corresponded with BLBP (*FABP7*)+cells on CN-spheroids (Fig. 4c, d) and CN tissues (Fig. 1h, i).

TAP gene upregulation is also supported by protein expression of EGFR, MASH (Fig. 4g), and SOX2 (Fig. 4h) on CN-spheroids. On the other hand, CN-differentiated cells showed upregulation of neuroblast genes, *ASPM* [63], *INA* [64] and *NRG1* [74] in comparison with CN-spheroids (Fig. 8a, b). This observation is corresponded well with the strong expression of PSA-NCAM and Tuj1 in CN tissues (Fig. 1c) and dissociated cells (Fig. 1e) at 1 week. Conversely, both CN-tumor spheres and SVZ-NSCs, were downregulated in expression of neuronal development related genes such as *FABP5* [75], *DIRAS* [76], *NEUROD1* [77], *NTF3* [78], *SLIT2* [79], *CD24* [80], *EMX1* [81], *STMN2* [82], *NRG1* [74], *RELN* [83], *HES6* [84], *L1CAM* [85], and *IGF2* [86], and the choroid plexus genes *AQP1* [87] and *EPHB2* (Fig. 8b) [88]. In particular, *CSPG2* [71], *CHL1* [46, 89], and *OLIG1* [19] were significantly upregulated in both CN-spheroids and SVZ-NSCs as compared to CN-differentiated cells (Fig. 7e). CHL1 is expressed and functions as a malignancy promoter in glioma cells [89]. Among the CSPG family genes, *CSPG2* was most strikingly upregulated in CN-spheroids as compared to their differentiated cells. Increased versican (*CSPG2*) expression is often observed in brain tumor growth [90].

In regard to tumorigenesis, both CN-tumor spheres and CN-differentiated cells showed an increase in expression of the embryonic oncogenesis-related genes: *NET1* [91], *MET* [92], *CD274* [93], and *WNT2* [94], and the proliferation related genes *FGF2* [78], *EGF* [20], *EGFL6* [95], and *TGBI* (Fig. 7d). In contrast, they showed a decrease in expression of genes related to tumor suppression and negative control of proliferation, namely *DIRAS1* [96], *CXXC4* [97], *EFNB2* [98], and *EFNB3* [98] (Fig. 8).

Differentiation potential of the CN-derived cells in vivo

We next assessed the bipotentiality of ITSFn-cultured cells *in vivo* by evaluating their fate after engraftment to immune-deficient NOD-SCID mouse. CN cells (1×10^5) were transplanted adjacent to the SVZ four weeks after primary culture to assess their lineage potential after transplantation. The recipients were sacrificed and fixed four weeks after transplantation. Human donor cells were identified by immunofluorescence of brain sections to detect human nuclear antigen (hNA) and DiI. Immunofluorescence analysis showed the presence of hNA+ cells in the grafts, demonstrating survival of grafted cells in the brain after transplantation (Fig. 9a, g). Most of the DiI+ CN-derived cells grafted in the striatum near SVZ were PSA-NCAM+ (64.00±3.786%, N=3) or Tuj1+ (75.67±2.333%, N=3) whereas fewer cells (17.00±2.082%, N=3%) were hNestin+ (Fig. 9b~f, k). Majority of Tuj1+ cells showed weak expression of GFAP (73.67±2.333% N=3), and this implicates these cells are differentiated from GFAP+/Tuj1+ TAPs. The PSA-NCAM+ cells displayed morphology similar to that of migrating neuroblasts (Fig. 9c). In contrast, most of the fetal brain-derived SNSCs grafted in the striatum near SVZ were Nestin+

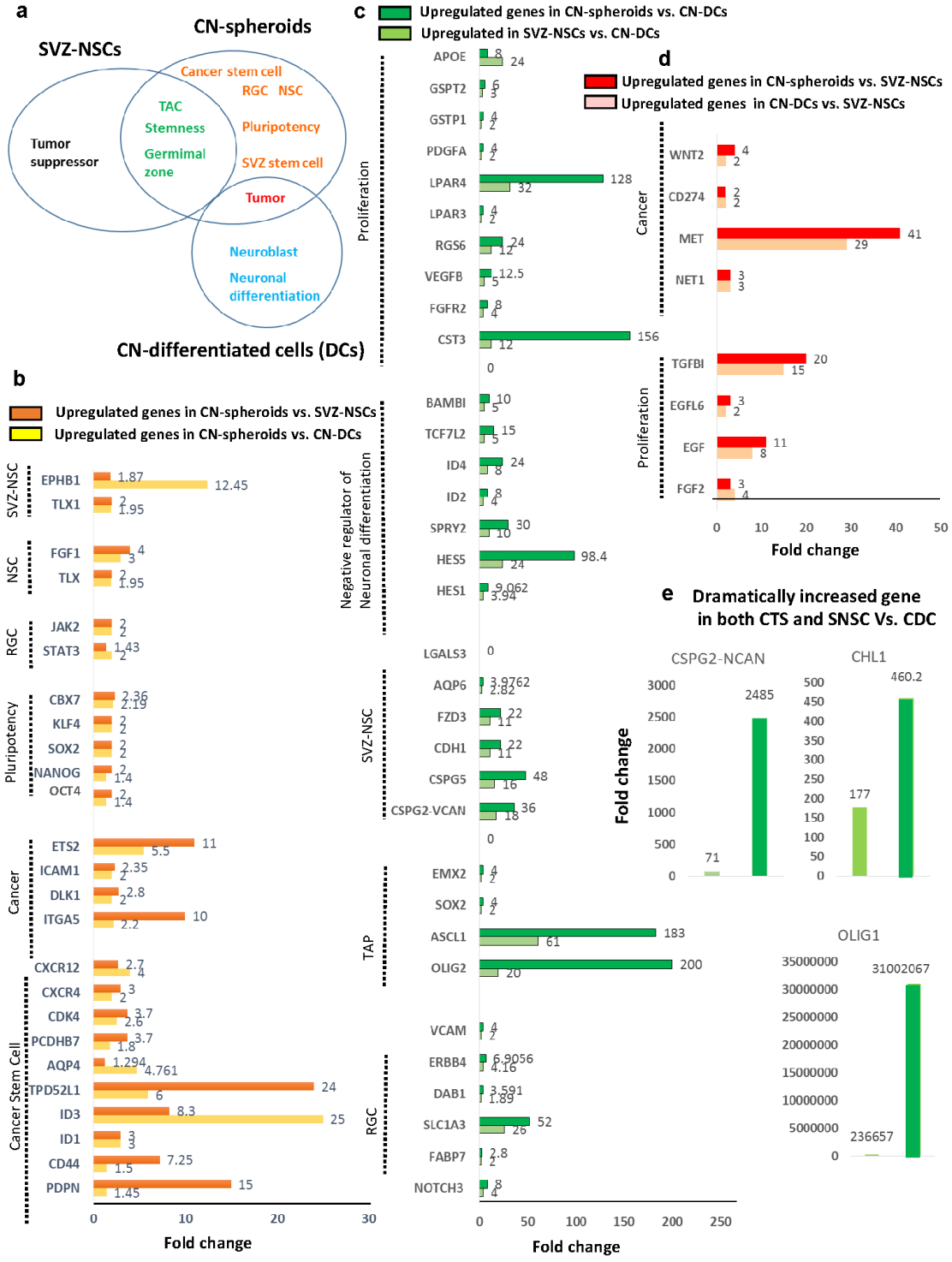

Fig. 7. Analysis of differential gene expression shows TAP- and RGC-like characteristics of CN spheroids from aggressive form of CN and their up-regulation of cancer stem cell genes. (a) Schematic showing overlap of genes in each category that are upregulated in SVZ-NSCs, CN-spheroids, and CN-differentiated cells. (b) Genes that are upregulated in CN-spheroids as compared to both SVZ-NSCs and CN- differentiated cells. Orange: Upregulated genes in CN-Spheroids vs SVZ-NSCs. Yellow: Upregulated genes in CN-Spheroids vs CN-differentiated cells. (c) Genes that are upregulated in CN-spheroids or SVZ-NSCs in comparison with CN-differentiated cells. Green: Upregulated genes in CN-Spheroids vs CN-differentiated cells. Light green: Upregulated genes in SVZ-NSCs vs CN-differentiated cells. (d) Genes that are upregulated in CN-spheroids or CN-differentiated cells in comparison with SVZ-NSCs. Orange: Upregulated genes in CN-Spheroids vs SVZ-NSCs. Peach: Upregulated genes in CN-differentiated cells vs SVZ-NSCs. (e) Dramatically upregulated genes in both CN-Spheroids and SVZ-NSCs vs CN-differentiated cells. One sample of CN-spheroids (N=1), CN-differentiated cells (N=1), and SVZ-NSCs (N=1) respectively analyzed.

https://doi.org/10.5607/en21004

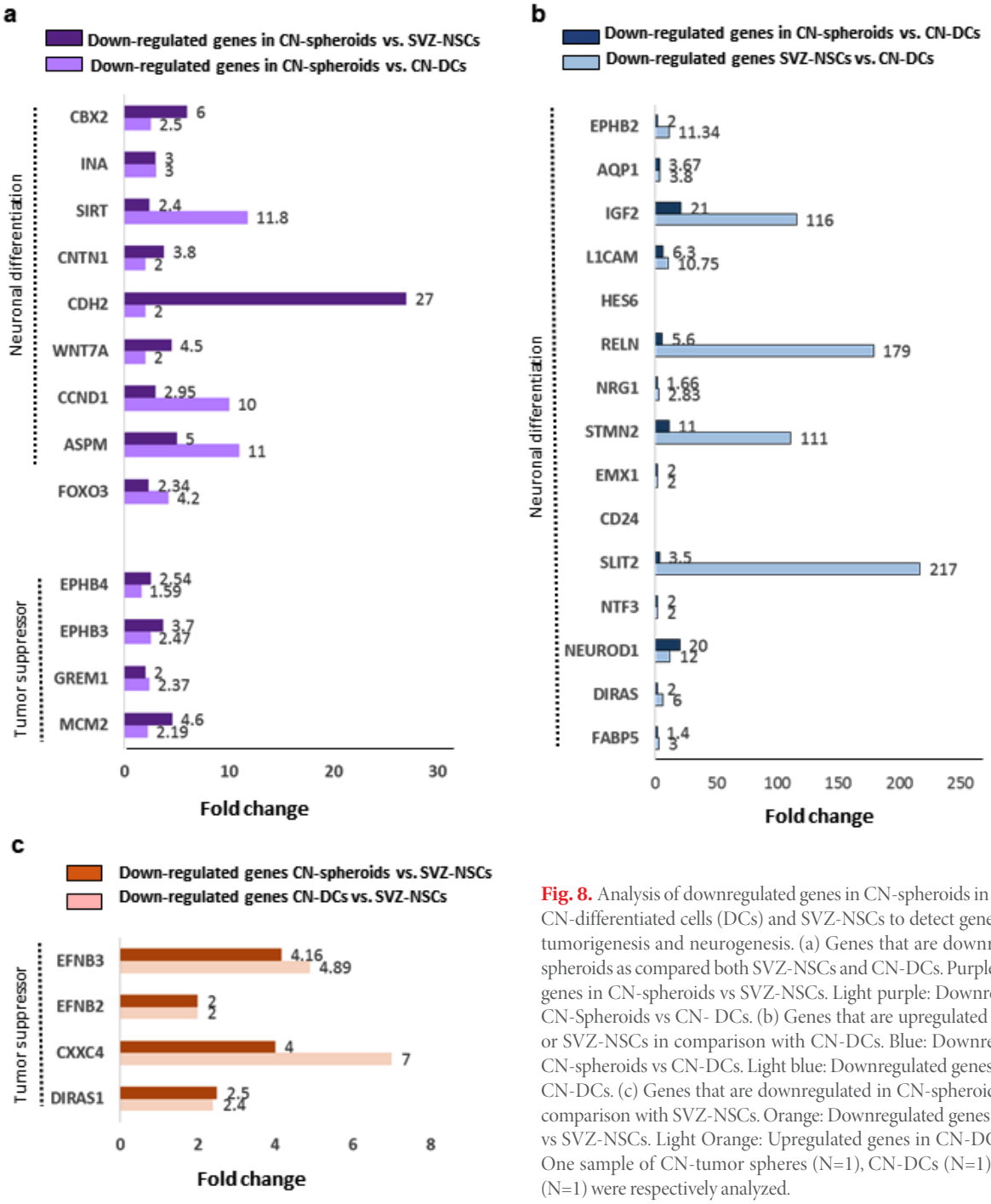

Fig. 8. Analysis of downregulated genes in CN-spheroids in comparison with CN-differentiated cells (DCs) and SVZ-NSCs to detect genes associated with tumorigenesis and neurogenesis. (a) Genes that are downregulated in CN-spheroids as compared both SVZ-NSCs and CN-DCs. Purple: Downregulated genes in CN-spheroids vs SVZ-NSCs. Light purple: Downregulated genes in CN-Spheroids vs CN- DCs. (b) Genes that are upregulated in CN-spheroids or SVZ-NSCs in comparison with CN-DCs. Blue: Downregulated genes in CN-spheroids vs CN-DCs. Light blue: Downregulated genes in SVZ-NSCs vs CN-DCs. (c) Genes that are downregulated in CN-spheroids or CN-DCs in comparison with SVZ-NSCs. Orange: Downregulated genes in CN-spheroids vs SVZ-NSCs. Light Orange: Upregulated genes in CN-DCs vs SVZ-NSCs. One sample of CN-tumor spheres (N=1), CN-DCs (N=1), and SVZ-NSCs (N=1) were respectively analyzed.

(89.67±3.528% N=3), and very few cells were Tuj1+ (12.67±2.333 N=3) (Fig. 9h~j, l). Taken together, the data suggest that, in this experimental context, cell fate is determined more by intrinsic factors than by the environmental niche up to 4 weeks.

DISCUSSION

In this study, we demonstrated SVZ-neurogenic cell composition in CN tissue and primary cells. Majority of CN cells have neuroblast characteristics, and its spheroids possess TAP and RGC-like characteristics based on their gene and protein marker expressions. First we showed that CN tissue and CN-derived cells

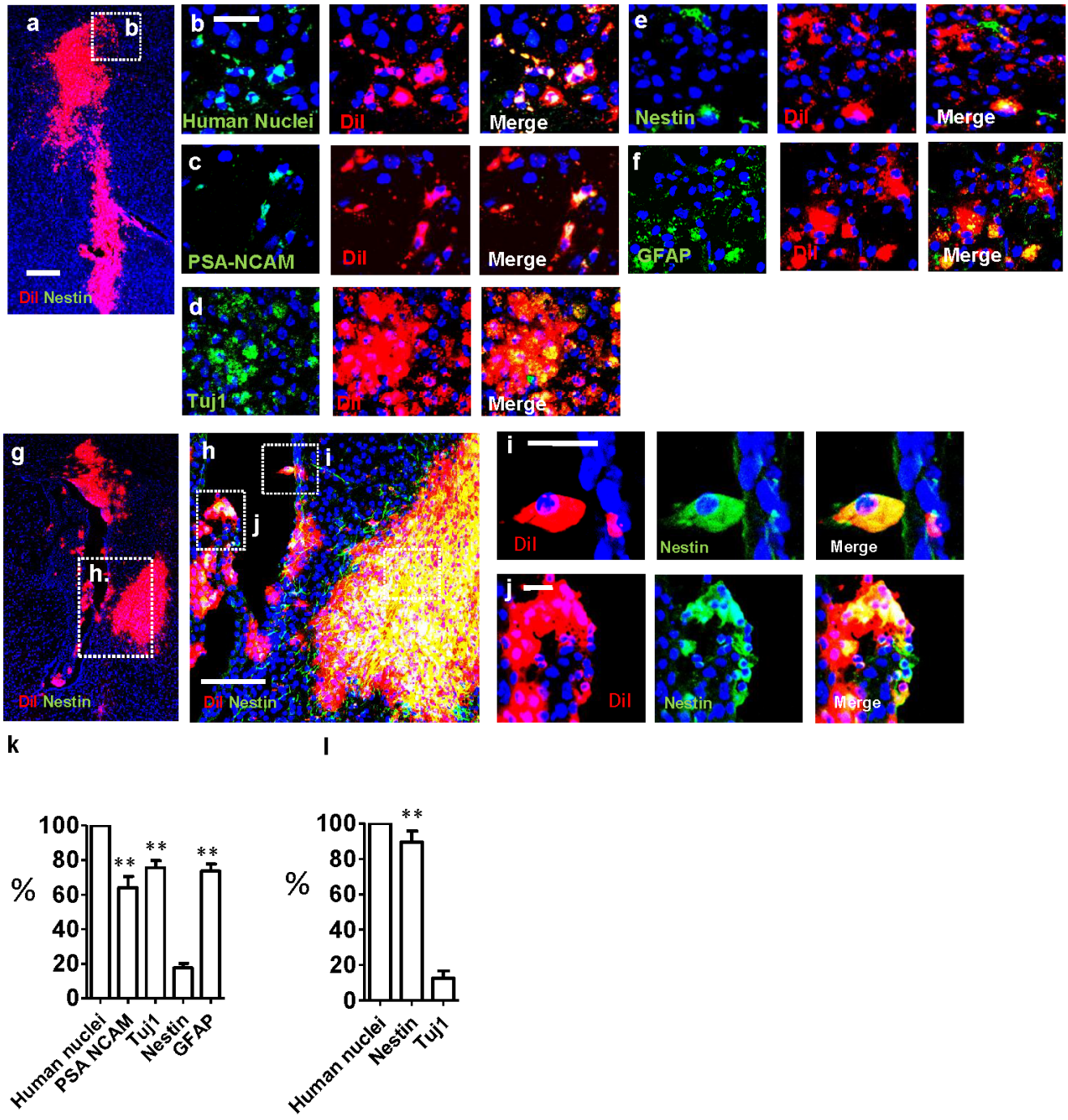

Fig. 9. Immunofluorescence analysis of CN cells engrafted into striatum of immune-deficient NOD-SCID mice. (a) Low power image of the grafted area showing DiI-labeled CN cells four weeks after engraftment. (b) Expression of hNA+ in DiI+ cells, confirming that DiI+ cells are from the CN-derived cells, not a result of contamination from the dye. (c~f) Immunofluorescence staining of CN-derived cells engrafted in the striatum near the SVZ, showing Tuj1+, PSA-NCAM+, GFAP+, and PSA-NCAM+ cells have morphology of migrating neuroblasts. (g) DiI-labeled fetal brain-derived SNSCs four weeks after engraftment in low power image. (h~i) Immunofluorescence staining of fetal brain-derived SNSCs grafted in the striatum near the SVZ shows that a majority of the cells are Nestin+. (h, l) Cellular composition of the CN-derived cells (h) and fetal brain-derived SNSCs (l), four weeks after engraftment in the striatum near the SVZ, respectively. Most of the DiI+ CN cells were PSA-NCAM+ or Tuj1+, whereas fewer cells were hNestin+ (h). Meanwhile, most of the fetal brain-derived SNSCs grafted in the striatum near SVZ were Nestin+, and very few cells were Tuj1+ (l). One-Way ANOVA analysis, ** ($p<0.05$) compared to Nestin (h) and Tuj1 (l). Scale bar, 50 μm (b~f) 100 μm (h) 25 μm (i, j). Three animals (N=3) were analyzed.

https://doi.org/10.5607/en21004

are comprised of three kinds of cells: GFAP-delta+, GFAP-delta+/Tuj1+, and Tuj1+ cells. The presence of GFAP-delta+/Tuj1+ cells is supported by an earlier study showing that the major population of GFAP+ proliferating cells were Tuj1-negative in the early SVZ, but Tuj1-positive in the adult SVZ, suggesting a decrease in postnatal neurogenesis occurs during development [99]. We hypothesize that GFAP-delta+, GFAP-delta+/Tuj1+, and Tuj1+ cells in CN correspond with NSCs, TAPs, and neuroblasts respectively, and CN-spheroids are a mixture of NSCs and TAPs, and that the majority of CN-differentiated cells are neuroblasts. In support of that hypothesis, we observed an upregulation of *EPHB1* expression in CN-spheroids, which supports an NSC identity, whereas upregulation of *EPHB2* in the CN-differentiated cells is consistent with neuroblast characteristics. This finding is supported by a previous report showing that EphB1 is expressed in SVZ astrocytes and that EphB2 is expressed Tuj1+ neuroblasts [88]. In consistent with the previous study which revealed that cell size decreases significantly from astroglial NSCs to TAPs or neuroblasts *in vivo* [22] , we observed that NSC-like GFAP-delta+ cells had elongated cell bodies with long process, and that TAP-like GFAP-delta+/Tuj1+ had an enlarged cell body with processes. Conversely, Tuj1+/PSA-NCAM neuroblasts have a round shaped morphology without mature neuronal structures, and they have the smallest cell body size. Although CN has been known as neuronal tumor, we observed that majority of CN cells express a neuroblast-associated PSA-NCAM, and DEG analysis showed upregulation of neuroblast genes, *ASPM* [63], *INA* [64] and *NRG1* [74] in CN-differentiated cells when compared with CN-spheroids.

On the other hand, CN-spheroids showed more pronounced TAP-characteristics compared to SVZ-NSC, suggesting that these TAP-like cells may function as tumor stem cells of CN. First DEG analysis showed a notable expression of *MASH1* [19], *EGFR* [20] and *SOX2* [21], which are key markers for TAPs, on CN-spheroids in comparison with SVZ-NSC, and their expression on CN-spheroids is also confirmed by immunostaining and RT-PCR. The TAP characteristics of CN-spheroids is further supported by our observation that TAP-specific genes, *OLIG1* [19], *OLIG2* [19], and *EMX2* [70] are upregulated in CN-spheroids, as compared to their differentiated cells. In particular GSEA analysis also showed that gene sets of EGFR signal are enriched in CN-spheroids in comparison with CN-differentiated cells. Our results are supported by the previous report Doetsch et al. [22], 2000, which revealed that the majority of EGF-responsive cells producing neurospheres *in vivo* are not derived from relatively quiescent NSC, but from the highly mitotic TAPs, and that TAPs maintain high levels of EGFR expression, perhaps related to their rapid division, and neuroblasts downregulate expression of the EGFR [22]. CN-spheroids also upregulated the gene sets of CSPG signaling such as *CSPG2* (*VCAN*), *CSPG3* (*NCAN*), and *CSPG5* [71] which stimulate NSC survival through enhanced EGFR signaling [100]. We speculate that CN tumor stem cells have TAP characteristics, and EGFR signaling has a critical role in tumorigenesis or spheroid formation of CN (Fig. 10), and that their ephemeral nature of TAPs, destined to neuroblast, might reflect benign characteristics of CN.

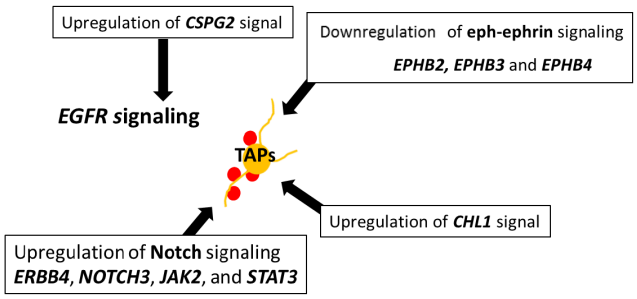

Fig. 10. Schematic summary of the key gene sets which presumably cause tumorigenesis of CN spheroids. CN-spheroids show upregulation of EGFR signaling, CSPG signaling, and Notch signaling, whereas eph-ephrin signaling is downregulated. CSPGs stimulate NSC survival through enhanced EGFR signaling. ERBB4 of Notch signaling is also function as oncogene. Eph-ephrin signaling, which is comprised with *EPHB2*, *EPHB3* and *EPHB4*, are known as putative tumor suppressor genes. CHL1 is expressed and functions as a malignancy promoter in GBM cells.

Meanwhile, a downregulation of putative tumor suppressor genes, *EPHB2*, *EPHB3* and *EPHB4* of eph-ephrin signaling [55-57] in CN-spheroids could also induce tumorigenesis of CN. This hypothesis is supported by the early study which shows that breakdown of *EPHB2* signaling results in invasion of SVZ astrocytes into the ependymal layer, which is accompanied by bulbous hyperplasia's along the lateral ventricle [98]. Similarly, the *EphrinB3*–/– mouse showed an increase in NPC proliferation and the presence of more neurosphere-forming NPCs in the developing SVZ [101]. Further supporting the RGC characteristics of CN-spheroids, we found that in CN-spheroids and SVZ-derived NSCs, the *NOTCH3* [65] coupled genes *FABP7* [66] (BLBP) and *DAB1* [67], *SLC1A3* (*GLAST*) [66], *VCAM* [69], and *ERBB4* [68] were upregulated. Interestingly, the *ERBB4* oncogene, which is expressed at high levels in EP and is associated with increased tumor-proliferative capacity, is an important target of NOTCH signaling in RGC [102]. Most strikingly, *IGF2* was downregulated 20- and 116-fold in CN-spheroids and SVZ-derived NSCs, respectively, as compared to CN-differentiated cells. Although *IGF2* has been reported to also be important for the proliferation of MB cells [103], and the findings of Sim et al. [5], suggested that the dysregulated autocrine signaling by *IGF2* contributes significantly to the genesis and expansion of neurocytoma, our findings suggest that *IGF2* is more likely to be involved in neurogenesis than in NSC prolifera-

tion [5]. Our result is supported by a previous study reporting that knockdown of *IGF2 in vitro* or within the adult SVZ does not affect NSC proliferation, and *IGF2* is strongly expressed in subsets of immature neuroblastoma cells [86], which correspond to the neuroblast-like CN-derived cells in our study.

CN is itself a rare tumor, and the aggressive form of CN is even rarer. Due to its rarity, this study might be more meaningful for the understanding of signaling and microenvironment which make aggressiveness of the tumor. In this study, all three samples made tumor spheres and all expressed cancer stem cell-specific markers, and one of the three samples, particularly, made notable number of tumor spheres. This observation reflects of variance among same diseases or heterogeneity of the individuals. And our observation of aggressive form of CN corresponds with one case report which addressed that some of aggressive form of CN progressed to glioma [3]. Intriguingly, MRI image of this case showed the size of Central neurocyoma is big which is full of the ventricular areas, and it is the same with the Patient 2 in our study. Signaling and gene expression of the rarely aggressive form of CN to our knowledge, have been never touched due to its scarcity. Here our study elucidates some enhanced genes in tumor spheroids of aggressive form CN which causes aggressiveness of this benign tumors. And these findings would give insightful information in searching for therapeutics of brain tumors.

In future study, it will be interesting to understand what intrinsic or micro-environmental factors contribute to their benign status compared with more aggressive tumors with similar gene expression profiles. Searching for genes that are differentially expressed in the aggressive tumor stem cells compared to CN tumor stem cells will be helpful for developing cancer targeted therapies.

In conclusion, here we show that tumor stem cells of CN possess TAP- and RGC-like characteristics with enhanced EGFR signaling which implicates its origin. In addition, by comparative DEG and GSEA analysis, we have identified CN spheroid genes that are consistent with a tumor stem cell function, as well as critical genes for NSC maintenance as well as neurogenesis. This research also provides innate neurogenesis signal, which is synchronized inartificially versus directed differentiation of human embryonic stem cells (hESCs) or induced pluripotent stem cells (iPSCs) into neurons.

ACKNOWLEDGEMENTS

This research was supported by the Korea Healthcare Technology R&D Project (grant no. HI11C21100200) of the Ministry of Health & Welfare, Republic of Korea; the Technology Innovation Program (grant no. 10050154, Business Model Development for Personalized Medicine Based on Integrated Genome and Clinical Information) of the Ministry of Trade, Industry & Energy (MI, Korea); the Bio & Medical Technology Development Program of the National Research Foundation (grant no. 2015M3C7A1028926) of the Ministry of Science and ICT, Republic of Korea; and the National Research Foundation of Korea Grant (grant no. NRF-2017M3C7A1047392) of the Ministry of Science and ICT, Republic of Korea to Sun Ha Paek.

REFERENCES

1. Smith AB, Smirniotopoulos JG, Horkanyne-Szakaly I (2013) From the radiologic pathology archives: intraventricular neoplasms: radiologic-pathologic correlation. Radiographics 33:21-43.
2. Chen CL, Shen CC, Wang J, Lu CH, Lee HT (2008) Central neurocytoma: a clinical, radiological and pathological study of nine cases. Clin Neurol Neurosurg 110:129-136.
3. Muragaki Y, Chernov M, Tajika Y, Kubo O, Iseki H, Hori T, Takakura K (2009) Coincidence of central neurocytoma and multiple glioblastomas: a rare case report. J Neurooncol 93:431-435.
4. Junttila MR, de Sauvage FJ (2013) Influence of tumour microenvironment heterogeneity on therapeutic response. Nature 501:346-354.
5. Sim FJ, Keyoung HM, Goldman JE, Kim DK, Jung HW, Roy NS, Goldman SA (2006) Neurocytoma is a tumor of adult neuronal progenitor cells. J Neurosci 26:12544-12555.
6. Paek SH, Shin HY, Kim JW, Park SH, Son JH, Kim DG (2010) Primary culture of central neurocytoma: a case report. J Korean Med Sci 25:798-803.
7. Hassoun J, Gambarelli D, Grisoli F, Pellet W, Salamon G, Pellissier JF, Toga M (1982) Central neurocytoma. An electron-microscopic study of two cases. Acta Neuropathol 56:151-156.
8. von Deimling A, Kleihues P, Saremaslani P, Yasargil MG, Spoerri O, Südhof TC, Wiestler OD (1991) Histogenesis and differentiation potential of central neurocytomas. Lab Invest 64:585-591.
9. Gage FH, Coates PW, Palmer TD, Kuhn HG, Fisher LJ, Suhonen JO, Peterson DA, Suhr ST, Ray J (1995) Survival and differentiation of adult neuronal progenitor cells transplanted to the adult brain. Proc Natl Acad Sci U S A 92:11879-11883.
10. Vescovi AL, Galli R, Reynolds BA (2006) Brain tumour stem cells. Nat Rev Cancer 6:425-436.
11. Singh SK, Hawkins C, Clarke ID, Squire JA, Bayani J, Hide T, Henkelman RM, Cusimano MD, Dirks PB (2004) Identifica-

tion of human brain tumour initiating cells. Nature 432:396-401.
12. Hemmati HD, Nakano I, Lazareff JA, Masterman-Smith M, Geschwind DH, Bronner-Fraser M, Kornblum HI (2003) Cancerous stem cells can arise from pediatric brain tumors. Proc Natl Acad Sci U S A 100:15178-15183.
13. Taylor MD, Poppleton H, Fuller C, Su X, Liu Y, Jensen P, Magdaleno S, Dalton J, Calabrese C, Board J, Macdonald T, Rutka J, Guha A, Gajjar A, Curran T, Gilbertson RJ (2005) Radial glia cells are candidate stem cells of ependymoma. Cancer Cell 8:323-335.
14. Gil-Perotin S, Marin-Husstege M, Li J, Soriano-Navarro M, Zindy F, Roussel MF, Garcia-Verdugo JM, Casaccia-Bonnefil P (2006) Loss of p53 induces changes in the behavior of subventricular zone cells: implication for the genesis of glial tumors. J Neurosci 26:1107-1116.
15. Doetsch F, García-Verdugo JM, Alvarez-Buylla A (1997) Cellular composition and three-dimensional organization of the subventricular germinal zone in the adult mammalian brain. J Neurosci 17:5046-5061.
16. Doetsch F, Caillé I, Lim DA, García-Verdugo JM, Alvarez-Buylla A (1999) Subventricular zone astrocytes are neural stem cells in the adult mammalian brain. Cell 97:703-716.
17. Alvarez-Buylla A, García-Verdugo JM, Tramontin AD (2001) A unified hypothesis on the lineage of neural stem cells. Nat Rev Neurosci 2:287-293.
18. Middeldorp J, Boer K, Sluijs JA, De Filippis L, Encha-Razavi F, Vescovi AL, Swaab DF, Aronica E, Hol EM (2010) GFAPdelta in radial glia and subventricular zone progenitors in the developing human cortex. Development 137:313-321.
19. Hack MA, Saghatelyan A, de Chevigny A, Pfeifer A, Ashery-Padan R, Lledo PM, Götz M (2005) Neuronal fate determinants of adult olfactory bulb neurogenesis. Nat Neurosci 865-872.
20. Cesetti T, Obernier K, Bengtson CP, Fila T, Mandl C, Hölzl-Wenig G, Wörner K, Eckstein V, Ciccolini F (2009) Analysis of stem cell lineage progression in the neonatal subventricular zone identifies EGFR+/NG2- cells as transit-amplifying precursors. Stem Cells 27:1443-1454.
21. Mu Y, Lee SW, Gage FH (2010) Signaling in adult neurogenesis. Curr Opin Neurobiol 20:416-423.
22. Doetsch F, Petreanu L, Caille I, Garcia-Verdugo JM, Alvarez-Buylla A (2002) EGF converts transit-amplifying neurogenic precursors in the adult brain into multipotent stem cells. Neuron 36:1021-1034.
23. van Strien ME, van den Berge SA, Hol EM (2011) Migrating neuroblasts in the adult human brain: a stream reduced to a trickle. Cell Res 21:1523-1525.
24. Lim DA, Tramontin AD, Trevejo JM, Herrera DG, García-Verdugo JM, Alvarez-Buylla A (2000) Noggin antagonizes BMP signaling to create a niche for adult neurogenesis. Neuron 28:713-726.
25. Shin HY, Hong YH, Jang SS, Chae HG, Paek SL, Moon HE, Kim DG, Kim J, Paek SH, Kim SJ (2010) A role of canonical transient receptor potential 5 channel in neuronal differentiation from A2B5 neural progenitor cells. PLoS One 5:e10359.
26. Shin HY, Kim JH, Phi JH, Park CK, Kim JE, Kim JH, Paek SH, Wang KC, Kim DG (2008) Endogenous neurogenesis and neovascularization in the neocortex of the rat after focal cerebral ischemia. J Neurosci Res 86:356-367.
27. Jeon YK, Park K, Park CK, Paek SH, Jung HW, Park SH (2007) Chromosome 1p and 19q status and p53 and p16 expression patterns as prognostic indicators of oligodendroglial tumors: a clinicopathological study using fluorescence in situ hybridization. Neuropathology 27:10-20.
28. Subramanian A, Tamayo P, Mootha VK, Mukherjee S, Ebert BL, Gillette MA, Paulovich A, Pomeroy SL, Golub TR, Lander ES, Mesirov JP (2005) Gene set enrichment analysis: a knowledge-based approach for interpreting genome-wide expression profiles. Proc Natl Acad Sci U S A 102:15545-15550.
29. Liberzon A, Subramanian A, Pinchback R, Thorvaldsdóttir H, Tamayo P, Mesirov JP (2011) Molecular signatures database (MSigDB) 3.0. Bioinformatics 27:1739-1740.
30. Costa MR, Ortega F, Brill MS, Beckervordersandforth R, Petrone C, Schroeder T, Götz M, Berninger B (2011) Continuous live imaging of adult neural stem cell division and lineage progression in vitro. Development 138:1057-1068.
31. Liu Y, Namba T, Liu J, Suzuki R, Shioda S, Seki T (2010) Glial fibrillary acidic protein-expressing neural progenitors give rise to immature neurons via early intermediate progenitors expressing both glial fibrillary acidic protein and neuronal markers in the adult hippocampus. Neuroscience 166:241-251.
32. Ponti G, Obernier K, Guinto C, Jose L, Bonfanti L, Alvarez-Buylla A (2013) Cell cycle and lineage progression of neural progenitors in the ventricular-subventricular zones of adult mice. Proc Natl Acad Sci U S A 110:E1045-E1054.
33. Günther HS, Schmidt NO, Phillips HS, Kemming D, Kharbanda S, Soriano R, Modrusan Z, Meissner H, Westphal M, Lamszus K (2008) Glioblastoma-derived stem cell-enriched cultures form distinct subgroups according to molecular and phenotypic criteria. Oncogene 27:2897-2909.
34. Kobayashi S, Shimamura T, Monti S, Steidl U, Hetherington CJ, Lowell AM, Golub T, Meyerson M, Tenen DG, Shapiro GI,

Halmos B (2006) Transcriptional profiling identifies cyclin D1 as a critical downstream effector of mutant epidermal growth factor receptor signaling. Cancer Res 66:11389-11398.
35. Lazennec G, Richmond A (2010) Chemokines and chemokine receptors: new insights into cancer-related inflammation. Trends Mol Med 16:133-144.
36. Mehrmohamadi M, Liu X, Shestov AA, Locasale JW (2014) Characterization of the usage of the serine metabolic network in human cancer. Cell Rep 9:1507-1519.
37. Harris MA, Yang H, Low BE, Mukherjee J, Guha A, Bronson RT, Shultz LD, Israel MA, Yun K (2008) Cancer stem cells are enriched in the side population cells in a mouse model of glioma. Cancer Res 68:10051-10059.
38. Wang S, Zhan M, Yin J, Abraham JM, Mori Y, Sato F, Xu Y, Olaru A, Berki AT, Li H, Schulmann K, Kan T, Hamilton JP, Paun B, Yu MM, Jin Z, Cheng Y, Ito T, Mantzur C, Greenwald BD, Meltzer SJ (2006) Transcriptional profiling suggests that Barrett's metaplasia is an early intermediate stage in esophageal adenocarcinogenesis. Oncogene 25:3346-3356.
39. Verhaak RG, Hoadley KA, Purdom E, Wang V, Qi Y, Wilkerson MD, Miller CR, Ding L, Golub T, Mesirov JP, Alexe G, Lawrence M, O'Kelly M, Tamayo P, Weir BA, Gabriel S, Winckler W, Gupta S, Jakkula L, Feiler HS, Hodgson JG, James CD, Sarkaria JN, Brennan C, Kahn A, Spellman PT, Wilson RK, Speed TP, Gray JW, Meyerson M, Getz G, Perou CM, Hayes DN; Cancer Genome Atlas Research Network (2010) Integrated genomic analysis identifies clinically relevant subtypes of glioblastoma characterized by abnormalities in PDGFRA, IDH1, EGFR, and NF1. Cancer Cell 17:98-110.
40. Karpowicz P, Willaime-Morawek S, Balenci L, DeVeale B, Inoue T, van der Kooy D (2009) E-cadherin regulates neural stem cell self-renewal. J Neurosci 29:3885-3896.
41. Anastassiou D, Rumjantseva V, Cheng W, Huang J, Canoll PD, Yamashiro DJ, Kandel JJ (2011) Human cancer cells express slug-based epithelial-mesenchymal transition gene expression signature obtained in vivo. BMC Cancer 11:529.
42. Abbud RA, Kelleher R, Melmed S (2004) Cell-specific pituitary gene expression profiles after treatment with leukemia inhibitory factor reveal novel modulators for proopiomelanocortin expression. Endocrinology 145:867-880.
43. de Magalhães JP, Curado J, Church GM (2009) Meta-analysis of age-related gene expression profiles identifies common signatures of aging. Bioinformatics 25:875-881.
44. do Carmo A, Patrico I, Curz MT, Carvalheiro H, Oliveira CR, Lopes MC (2010) CXCL12/CXCR4 promotes motility and proliferation of glioma cells: Cancer Biology & Therapy 2010; 9: 56-65. Ann Neurosci 17:85-86.
45. Bockstaele L, Bisteau X, Paternot S, Roger PP (2009) Differential regulation of cyclin-dependent kinase 4 (CDK4) and CDK6, evidence that CDK4 might not be activated by CDK7, and design of a CDK6 activating mutation. Mol Cell Biol 29:4188-4200.
46. Buzhor E, Harari-Steinberg O, Omer D, Metsuyanim S, Jacob-Hirsch J, Noiman T, Dotan Z, Goldstein RS, Dekel B (2011) Kidney spheroids recapitulate tubular organoids leading to enhanced tubulogenic potency of human kidney-derived cells. Tissue Eng Part A 17:2305-2319.
47. Warth A, Simon P, Capper D, Goeppert B, Tabatabai G, Herzog H, Dietz K, Stubenvoll F, Ajaaj R, Becker R, Weller M, Meyermann R, Wolburg H, Mittelbronn M (2007) Expression pattern of the water channel aquaporin-4 in human gliomas is associated with blood-brain barrier disturbance but not with patient survival. J Neurosci Res 85:1336-1346.
48. Boutros R, Byrne JA (2005) D53 (TPD52L1) is a cell cycle-regulated protein maximally expressed at the G2-M transition in breast cancer cells. Exp Cell Res 310:152-165.
49. Castañon E, Bosch-Barrera J, López I, Collado V, Moreno M, López-Picazo JM, Arbea L, Lozano MD, Calvo A, Gil-Bazo I (2013) Id1 and Id3 co-expression correlates with clinical outcome in stage III-N2 non-small cell lung cancer patients treated with definitive chemoradiotherapy. J Transl Med 11:13.
50. Jaggupilli A, Elkord E (2012) Significance of CD44 and CD24 as cancer stem cell markers: an enduring ambiguity. Clin Dev Immunol 2012:708036.
51. Ernst A, Hofmann S, Ahmadi R, Becker N, Korshunov A, Engel F, Hartmann C, Felsberg J, Sabel M, Peterziel H, Durchdewald M, Hess J, Barbus S, Campos B, Starzinski-Powitz A, Unterberg A, Reifenberger G, Lichter P, Herold-Mende C, Radlwimmer B (2009) Genomic and expression profiling of glioblastoma stem cell-like spheroid cultures identifies novel tumor-relevant genes associated with survival. Clin Cancer Res 15:6541-6550.
52. Takahashi K, Yamanaka S (2006) Induction of pluripotent stem cells from mouse embryonic and adult fibroblast cultures by defined factors. Cell 126:663-676.
53. Morey L, Pascual G, Cozzuto L, Roma G, Wutz A, Benitah SA, Di Croce L (2012) Nonoverlapping functions of the Polycomb group Cbx family of proteins in embryonic stem cells. Cell Stem Cell 10:47-62.
54. Rusiniak ME, Kunnev D, Freeland A, Cady GK, Pruitt SC (2012) Mcm2 deficiency results in short deletions allowing high resolution identification of genes contributing to lymphoblastic lymphoma. Oncogene 31:4034-4044.

55. Kandouz M, Haidara K, Zhao J, Brisson ML, Batist G (2010) The EphB2 tumor suppressor induces autophagic cell death via concomitant activation of the ERK1/2 and PI3K pathways. Cell Cycle 9:398-407.
56. Schauer MC, Stoecklein NH, Theisen J, Kröpil F, Baldus S, Hoelscher A, Feith M, Bölke E, Matuschek C, Budach W, Knoefel WT (2012) The simultaneous expression of both ephrin B3 receptor and E-cadherin in Barrett's adenocarcinoma is associated with favorable clinical staging. Eur J Med Res 17:10.
57. Noren NK, Foos G, Hauser CA, Pasquale EB (2006) The EphB4 receptor suppresses breast cancer cell tumorigenicity through an Abl-Crk pathway. Nat Cell Biol 8:815-825.
58. Ahlenius H, Chanda S, Webb AE, Yousif I, Karmazin J, Prusiner SB, Brunet A, Südhof TC, Wernig M (2016) FoxO3 regulates neuronal reprogramming of cells from postnatal and aging mice. Proc Natl Acad Sci U S A 113:8514-8519.
59. Prajerova I, Honsa P, Chvatal A, Anderova M (2010) Distinct effects of sonic hedgehog and Wnt-7a on differentiation of neonatal neural stem/progenitor cells in vitro. Neuroscience 171:693-711.
60. Yagita Y, Sakurai T, Tanaka H, Kitagawa K, Colman DR, Shan W (2009) N-cadherin mediates interaction between precursor cells in the subventricular zone and regulates further differentiation. J Neurosci Res 87:3331-3342.
61. Khodosevich K, Seeburg PH, Monyer H (2009) Major signaling pathways in migrating neuroblasts. Front Mol Neurosci 2:7.
62. Ferrante RJ, Browne SE, Shinobu LA, Bowling AC, Baik MJ, MacGarvey U, Kowall NW, Brown RH Jr, Beal MF (1997) Evidence of increased oxidative damage in both sporadic and familial amyotrophic lateral sclerosis. J Neurochem 69:2064-2074.
63. Gonzalez C, Saunders RD, Casal J, Molina I, Carmena M, Ripoll P, Glover DM (1990) Mutations at the asp locus of Drosophila lead to multiple free centrosomes in syncytial embryos, but restrict centrosome duplication in larval neuroblasts. J Cell Sci 96 (Pt 4):605-616.
64. Levavasseur F, Zhu Q, Julien JP (1999) No requirement of alpha-internexin for nervous system development and for radial growth of axons. Brain Res Mol Brain Res 69:104-112.
65. Dang L, Yoon K, Wang M, Gaiano N (2006) Notch3 signaling promotes radial glial/progenitor character in the mammalian telencephalon. Dev Neurosci 28:58-69.
66. Anthony TE, Mason HA, Gridley T, Fishell G, Heintz N (2005) Brain lipid-binding protein is a direct target of Notch signaling in radial glial cells. Genes Dev 19:1028-1033.
67. Hartfuss E, Förster E, Bock HH, Hack MA, Leprince P, Luque JM, Herz J, Frotscher M, Götz M (2003) Reelin signaling directly affects radial glia morphology and biochemical maturation. Development 130:4597-4609.
68. Rio C, Rieff HI, Qi P, Khurana TS, Corfas G (1997) Neuregulin and erbB receptors play a critical role in neuronal migration. Neuron 19:39-50.
69. Kawaguchi A, Ikawa T, Kasukawa T, Ueda HR, Kurimoto K, Saitou M, Matsuzaki F (2008) Single-cell gene profiling defines differential progenitor subclasses in mammalian neurogenesis. Development 135:3113-3124.
70. Gangemi RM, Daga A, Marubbi D, Rosatto N, Capra MC, Corte G (2001) Emx2 in adult neural precursor cells. Mech Dev 109:323-329.
71. Tham M, Ramasamy S, Gan HT, Ramachandran A, Poonepalli A, Yu YH, Ahmed S (2010) CSPG is a secreted factor that stimulates neural stem cell survival possibly by enhanced EGFR signaling. PLoS One 5:e15341.
72. Preston M, Sherman LS (2011) Neural stem cell niches: roles for the hyaluronan-based extracellular matrix. Front Biosci (Schol Ed) 3:1165-1179.
73. Tissir F, Goffinet AM (2010) Planar cell polarity signaling in neural development. Curr Opin Neurobiol 20:572-577.
74. Ghashghaei HT, Weber J, Pevny L, Schmid R, Schwab MH, Lloyd KC, Eisenstat DD, Lai C, Anton ES (2006) The role of neuregulin-ErbB4 interactions on the proliferation and organization of cells in the subventricular zone. Proc Natl Acad Sci U S A 103:1930-1935.
75. Liu JW, Almaguel FG, Bu L, De Leon DD, De Leon M (2008) Expression of E-FABP in PC12 cells increases neurite extension during differentiation: involvement of n-3 and n-6 fatty acids. J Neurochem 106:2015-2029.
76. Wylie CJ, Hendricks TJ, Zhang B, Wang L, Lu P, Leahy P, Fox S, Maeno H, Deneris ES (2010) Distinct transcriptomes define rostral and caudal serotonin neurons. J Neurosci 30:670-684.
77. Boutin C, Hardt O, de Chevigny A, CoréN, Goebbels S, Seidenfaden R, Bosio A, Cremer H (2010) NeuroD1 induces terminal neuronal differentiation in olfactory neurogenesis. Proc Natl Acad Sci U S A 107:1201-1206.
78. Lukaszewicz A, Savatier P, Cortay V, Kennedy H, Dehay C (2002) Contrasting effects of basic fibroblast growth factor and neurotrophin 3 on cell cycle kinetics of mouse cortical stem cells. J Neurosci 22:6610-6622.
79. Li HS, Chen JH, Wu W, Fagaly T, Zhou L, Yuan W, Dupuis S, Jiang ZH, Nash W, Gick C, Ornitz DM, Wu JY, Rao Y (1999) Vertebrate slit, a secreted ligand for the transmembrane protein roundabout, is a repellent for olfactory bulb axons. Cell

96:807-818.
80. Pruszak J, Ludwig W, Blak A, Alavian K, Isacson O (2009) CD15, CD24, and CD29 define a surface biomarker code for neural lineage differentiation of stem cells. Stem Cells 27:2928-2940.
81. Chan CH, Godinho LN, Thomaidou D, Tan SS, Gulisano M, Parnavelas JG (2001) Emx1 is a marker for pyramidal neurons of the cerebral cortex. Cereb Cortex 11:1191-1198.
82. Xu H, Dhanasekaran DN, Lee CM, Reddy EP (2010) Regulation of neurite outgrowth by interactions between the scaffolding protein, JNK-associated leucine zipper protein, and neuronal growth-associated protein superior cervical ganglia clone 10. J Biol Chem 285:3548-3553.
83. Pesold C, Impagnatiello F, Pisu MG, Uzunov DP, Costa E, Guidotti A, Caruncho HJ (1998) Reelin is preferentially expressed in neurons synthesizing gamma-aminobutyric acid in cortex and hippocampus of adult rats. Proc Natl Acad Sci U S A 95:3221-3226.
84. Gratton MO, Torban E, Jasmin SB, Theriault FM, German MS, Stifani S (2003) Hes6 promotes cortical neurogenesis and inhibits Hes1 transcription repression activity by multiple mechanisms. Mol Cell Biol 23:6922-6935.
85. Poplawski GH, Tranziska AK, Leshchyns'ka I, Meier ID, Streichert T, Sytnyk V, Schachner M (2012) L1CAM increases MAP2 expression via the MAPK pathway to promote neurite outgrowth. Mol Cell Neurosci 50:169-178.
86. Mohlin S, Hamidian A, Påhlman S (2013) HIF2A and IGF2 expression correlates in human neuroblastoma cells and normal immature sympathetic neuroblasts. Neoplasia 15:328-334.
87. Zhang H, Verkman AS (2015) Aquaporin-1 water permeability as a novel determinant of axonal regeneration in dorsal root ganglion neurons. Exp Neurol 265:152-159.
88. Nomura T, Göritz C, Catchpole T, Henkemeyer M, Frisén J (2010) EphB signaling controls lineage plasticity of adult neural stem cell niche cells. Cell Stem Cell 7:730-743.
89. Yang Z, Xie Q, Hu CL, Jiang Q, Shen HF, Schachner M, Zhao WJ (2017) CHL1 is expressed and functions as a malignancy promoter in glioma cells. Front Mol Neurosci 10:324.
90. Paulus W, Baur I, Dours-Zimmermann MT, Zimmermann DR (1996) Differential expression of versican isoforms in brain tumors. J Neuropathol Exp Neurol 55:528-533.
91. Vessichelli M, Ferravante A, Zotti T, Reale C, Scudiero I, Picariello G, Vito P, Stilo R (2012) Neuroepithelial transforming gene 1 (Net1) binds to caspase activation and recruitment domain (CARD)- and membrane-associated guanylate kinase-like domain-containing (CARMA) proteins and regulates nuclear factor κB activation. J Biol Chem 287:13722-13730.
92. Wallace GC 4th, Dixon-Mah YN, Vandergrift WA 3rd, Ray SK, Haar CP, Mittendorf AM, Patel SJ, Banik NL, Giglio P, Das A (2013) Targeting oncogenic ALK and MET: a promising therapeutic strategy for glioblastoma. Metab Brain Dis 28:355-366.
93. Taube JM, Young GD, McMiller TL, Chen S, Salas JT, Pritchard TS, Xu H, Meeker AK, Fan J, Cheadle C, Berger AE, Pardoll DM, Topalian SL (2015) Differential expression of immune-regulatory genes associated with PD-L1 display in melanoma: implications for PD-1 pathway blockade. Clin Cancer Res 21:3969-3976.
94. Pu P, Zhang Z, Kang C, Jiang R, Jia Z, Wang G, Jiang H (2009) Downregulation of Wnt2 and beta-catenin by siRNA suppresses malignant glioma cell growth. Cancer Gene Ther 16:351-361.
95. Yeung G, Mulero JJ, Berntsen RP, Loeb DB, Drmanac R, Ford JE (1999) Cloning of a novel epidermal growth factor repeat containing gene EGFL6: expressed in tumor and fetal tissues. Genomics 62:304-307.
96. Ellis CA, Vos MD, Howell H, Vallecorsa T, Fults DW, Clark GJ (2002) Rig is a novel Ras-related protein and potential neural tumor suppressor. Proc Natl Acad Sci U S A 99:9876-9881.
97. Kojima T, Shimazui T, Hinotsu S, Joraku A, Oikawa T, Kawai K, Horie R, Suzuki H, Nagashima R, Yoshikawa K, Michiue T, Asashima M, Akaza H, Uchida K (2009) Decreased expression of CXXC4 promotes a malignant phenotype in renal cell carcinoma by activating Wnt signaling. Oncogene 28:297-305.
98. Conover JC, Doetsch F, Garcia-Verdugo JM, Gale NW, Yancopoulos GD, Alvarez-Buylla A (2000) Disruption of Eph/ephrin signaling affects migration and proliferation in the adult subventricular zone. Nat Neurosci 3:1091-1097.
99. Namba T, Mochizuki H, Suzuki R, Onodera M, Yamaguchi M, Namiki H, Shioda S, Seki T (2011) Time-lapse imaging reveals symmetric neurogenic cell division of GFAP-expressing progenitors for expansion of postnatal dentate granule neurons. PLoS One 6:e25303.
100. Sirko S, von Holst A, Weber A, Wizenmann A, Theocharidis U, Götz M, Faissner A (2010) Chondroitin sulfates are required for fibroblast growth factor-2-dependent proliferation and maintenance in neural stem cells and for epidermal growth factor-dependent migration of their progeny. Stem Cells 28:775-787.
101. Ricard J, Salinas J, Garcia L, Liebl DJ (2006) EphrinB3 regulates cell proliferation and survival in adult neurogenesis. Mol Cell Neurosci 31:713-722.

102. Gilbertson RJ, Bentley L, Hernan R, Junttila TT, Frank AJ, Haapasalo H, Connelly M, Wetmore C, Curran T, Elenius K, Ellison DW (2002) ERBB receptor signaling promotes ependymoma cell proliferation and represents a potential novel therapeutic target for this disease. Clin Cancer Res 8:3054-3064.
103. Corcoran RB, Bachar Raveh T, Barakat MT, Lee EY, Scott MP (2008) Insulin-like growth factor 2 is required for progression to advanced medulloblastoma in patched1 heterozygous mice. Cancer Res 68:8788-8795.